Ocean Carbon Uptake Under Aggressive Emission Mitigation

Sean Ridge[1] and Galen A. McKinley[1]

[1]Columbia University and Lamont Doherty Earth Observatory, New York, United States

Correspondence: (Galen A. McKinley, mckinley@ldeo.columbia.edu)

Abstract. Nearly every nation has signed the UNFCC Paris Agreement, committing to mitigate ~~global~~ anthropogenic carbon emissions ~~and~~ so as to limit global mean temperature increase to no more than 1.5°C. A consequence of emission mitigation that has received limited attention is a reduced efficiency of the ocean carbon sink. Historically, the roughly exponential increase of atmospheric CO_2 has resulted in a proportional increase in anthropogenic carbon uptake by the ocean. We define growth of the ocean carbon sink exactly proportional to the atmospheric growth rate to be 100% efficient. Using a model hierarchy consisting of a ~~standard one-dimensional~~ common reduced-form ocean carbon cycle model and ~~a complex~~ the Community Earth System Model (~~ESM~~CESM), we ~~compare the future efficiency change~~ assess the mechanisms of future change in the efficiency of the ocean carbon sink ~~in response to aggressive emission~~ under three emission scenarios: aggressive mitigation (1.5°C), intermediate ~~emission~~ mitigation (RCP4.5), and ~~no emission mitigation~~ high emissions (RCP8.5). The ~~one-dimensional~~ reduced-form ocean carbon cycle model ~~, which is designed to replicate~~ is tuned to emulate the global-mean behavior of the ~~ESM, demonstrates that growth of ocean anthropogenic carbon uptake is a balance between enhancement due to a positive atmospheric growth rate, and decreases due to the positive growth rate of dissolved in the surface ocean. Without emission mitigation (~~CESM, and then allows for mechanistic decomposition. With intermediate or no mitigation (RCP4.5, RCP8.5), changes in efficiency through 2080 are almost entirely the result of ~~changes in the~~ future reductions in the carbonate buffer capacity of the ocean~~, which accelerates the growth rate of dissolved in the surface ocean~~. Under the ~~declining regime of the~~ 1.5°C scenario, the dominant driver of efficiency decline is the ~~carbon gradient effect, in which the anthropogenic carbon already present in the near-surface ocean slows down further removal of anthropogenic carbon~~ ocean's reduced ability to transport anthropogenic carbon from surface to depth. As the global-mean upper-ocean gradient of anthropogenic carbon reverses sign, carbon can be re-entrained in surface waters where it slows further removal from the atmosphere. Reducing uncertainty in ~~the circulation of the upper ocean~~ ocean circulation is critical to ~~improving quantification of the carbon gradient effect and~~ better understanding the transport of anthropogenic carbon from surface to depth, and to improving quantification of its role in the future ocean carbon sink~~under emissions mitigation~~.

1 Introduction

The ocean has absorbed excess carbon equivalent to 39% of the CO_2 from industrial era fossil fuel combustion and cement production (Friedlingstein et al., 2019). The rest of the CO_2 remains in the atmosphere where it acts as the primary driver of climate change. At the global scale, the partial pressure of CO_2 in the atmosphere (pCO_2^{atm}) is greater than the partial

pressure of CO_2 in the surface ocean (pCO_2^{ocn}), thus there is a net ocean sink. The difference in partial pressures has grown over time, therefore ocean uptake of atmospheric CO_2 has increased over the industrial era (Khatiwala et al., 2009; DeVries, 2014). The carbon that has been added to the ocean and atmosphere as the result of anthropogenic CO_2 emissions is referred to as anthropogenic carbon, C_{ant}.

The rate of ocean anthropogenic carbon uptake is further controlled by carbon chemistry in seawater and physical removal of anthropogenic carbon from the surface ocean into the ocean interior (Graven et al., 2012). Various processes set the rate of ~~physical anthropogenic carbon removal~~ transport from surface to depth of anthropogenic carbon (Bopp et al., 2015; Gnanadesikan et al., 2015; Iudicone et al., 2016). Advection and watermass transformation dominates regional patterns of anthropogenic carbon fluxes into (reemergence) and out of (subduction) the seasonal mixed layer (Bopp et al., 2015; Iudicone et al., 2016; Toyama et al., 2017). However, large positive and negative signs of these fluxes mostly cancel when globally integrated (Bopp et al., 2015)~~and thus do not play a dominant role in setting the globally integrated air-sea flux of anthropogenic carbon. By setting an appropriate value of an effective surface diffusivity ($K_{z,eff}$) to parameterize removal as a simple diffusive process, it has been shown that one-dimensional models can simulate an~~ , and thus can be conceptualized as a diffusive process in a vertical column (Section 2.4). By parameterizing the ocean's global-mean removal of carbon to depth as a constant process, models based on an impulse response function (IRF) can replicate ocean anthropogenic carbon uptake that is quantitatively consistent with the ~~ocean anthropogenic carbon~~ uptake of complex models and observations (Oeschger et al., 1975; Joos et al., 1996).

~~Efficiency~~ The efficiency of land and ocean sinks may be described by the CO_2 sink rate (k_S; Raupach et al. (2014)), which is the combined ocean-land CO_2 uptake per unit atmospheric CO_2 above preindustrial levels (C_{ant}^{ATM}, PgC):

$$k_S(t) = \frac{F_{ant}^L(t) + F_{ant}^M(t)}{C_{ant}^{ATM}(t)} \tag{1}$$

Where F_{ant}^L (Pg C yr^{-1}) is the anthropogenic land sink and F_{ant}^M (Pg C yr^{-1}) is the anthropogenic ocean sink.

Observations of k_S from 1959-2012 indicate a robust declining trend, and thus the rate of increase in the ~~natural~~ sinks has been slower than the accumulation of carbon in the atmosphere (Canadell et al., 2007; Raupach et al., 2014). ~~This result is as expected because the theoretical prediction of constant sink efficiency is only valid if emissions are strictly exponential.~~ Raupach et al. (2014) illustrate that the observed declining k_S is attributable to this slower-than-exponential CO_2 emissions growth (~35% of the trend), a decline in ~~the size of~~ major volcanic eruptions, which cause brief periods of global cooling (~25%), response of the natural sinks to a warming climate (~20%), and nonlinear responses to increasing atmospheric CO_2 (mostly attributable to ocean chemistry; ~20%).

The contribution of ocean anthropogenic carbon uptake to k_S is k_M:

$$k_M(t) = \frac{F_{ant}^M(t)}{C_{ant}^{ATM}(t)} \tag{2}$$

If there is exponentially increasing pCO_2^{atm}, and constant gas solubility, air-sea transfer coefficient, and carbonate buffer capacity, theory indicates that k_M will remain constant (Raupach et al., 2014). Because these conditions do approximately describe historical conditions, constant proportionality for ocean anthropogenic carbon uptake has been used as a null hypothesis

in studies of the drivers of historical regional and global scale changes in the ocean carbon cycle (Lovenduski et al., 2008; Gruber et al., 201
. Here we refer to this constant proportionality (i.e. $k_M = constant$) as the "historical scaling". The term often used is "the transient steady state assumption" (Gammon et al., 1982; Tanhua et al., 2007; Lovenduski et al., 2008; Gruber et al., 2019). We choose "historical scaling" to clarify that this null hypothesis was appropriate for the last several decades of the 20th century, and to allow for emphasis on the fact that this assumption should be increasingly less accurate going forward.

Slowing of the emissions growth rate, and thus the pCO_2^{atm} growth rate, reduces the efficiency of k_M (McKinley et al., 2020; Raupach et (Raupach et al., 2014; McKinley et al., 2020). A central motivation for this work is the fact thatthe future , in the future, a reduced pCO_2^{atm} growth rate is inevitable, due either to climate policy (Hausfather and Peters, 2020) , or by or to the eventual exhaustion of fossil fuel reservoirs.

In addition to k_M efficiency changes due to slowing pCO_2^{atm} growth rate, there will also be impacts on k_M from climate-carbon carbon cycle feedbacks (Friedlingstein et al., 2013; Raupach et al., 2014). Past studies have separated carbon cycle feedbacks into CO_2 concentration effects and climate driven effects (Friedlingstein et al., 2013; Arora et al., 2013). Climate driven effects stem from the warming of the surface ocean, which reduces gas solubility and slows the ocean circulation, thus reducing the efficiency of ocean uptake (Friedlingstein et al., 2013). The CO_2 concentration effect in the ocean is has typically been thought of as the net result of two effects: increased flux driven by increasing pCO_2^{atm} and reduced flux due to declining buffer capacity. The buffering capacity of the ocean refers to the transfer of absorbed CO_2 via chemical reactions into chemical species that do not exchange with the atmosphere. As more CO_2 is added to the ocean, buffer capacity decreases (Fassbender et al., 2017). When buffer capacity is reduced, more of the CO_2 remains in a form that can exchange with the atmosphereand , and thus the efficiency of ocean anthropogenic carbon uptake declines. Schwinger and Tjiputra (2018) illustrate that for scenarios of emission mitigation, there is also an important additional component to the CO_2 concentration feedback. Because the ocean only slowly transports CO_2 from surface to depth, when emissions are mitigated, the elevated CO_2 concentration of the upper ocean acts to slow additional carbon uptake. We explore this feedback under more realistic forcing scenarios in this study.

Climate driven effects stem from the warming of the surface ocean, which reduces gas solubility, and ocean circulation. Projected warming reduces ocean uptake (Friedlingstein et al., 2013) and thus reduces the efficiency of ocean uptake. Impacts of warming on future carbon uptake have been quantified using a climate feedbackframework (Friedlingstein et al., 2013; Randerson et al.,
. However, the simulations used in these studies have not allowed for separation of the effects due to buffering capacity.

Under exponentially increasing , constant gas solubility, and constant chemical capacity, theory indicates that k_M will remain constant (Raupach et al., 2014). Because these conditions do approximately describe the historical conditions of the ocean carbon cycle, constant proportionality for ocean anthropogenic carbon uptakehas been used as a null hypothesis in studies of the drivers of historical regional and global scale changes in the ocean carbon cycle (Lovenduski et al., 2008; Gruber et al., 2019)
. Here we refer to this constant proportionality (i.e. $k_M = constant$) as the "historical scaling". The term often used is "the transient steady state assumption" (Gammon et al., 1982; Tanhua et al., 2007; Lovenduski et al., 2008; Gruber et al., 2019). We choose "historical scaling" to clarify that this null hypothesis was appropriate for the last several decades of the 20th century, and to allow for emphasis on the fact that this assumption should be increasingly less accurate going forward.

This work expands upon previous work that has quantified future change in ocean anthropogenic carbon uptake. We separately account for changes due to buffering ~~, circulation~~ and the future trajectory of pCO_2^{atm}, and therefore, by residual, we are able to estimate the degree to which carbon already held in the upper ocean will slow the sink. We compare ~~a future scenario with moderate levels of~~ future scenarios with high emissions (RCP8.5), intermediate mitigation (RCP4.5; Meinshausen et al. (2011)) and an aggressive mitigation scenario where the 1.5°C target is met (1.5°C; Sanderson et al. (2017)) ~~to the standard business-as-usual RCP8.5~~ using ensemble results from an Earth System ~~model~~ Model (ESM). ~~In the RCP8.5 scenario (Meinshausen et al., 2011), increases nearly exponentially.~~ We use a ~~one-dimensional~~ reduced-form ocean carbon cycle model to emulate the ESM for each scenario, and with ~~this one-dimensional model, we~~ it, diagnose the mechanisms of ocean carbon sink efficiency decline in the future projections. We determine for the three pCO_2^{atm} scenarios how reduced buffering~~and the~~, warming impacts on carbon solubility and a steady circulation interacting with a changing surface to depth gradient of anthropogenic carbon should impact ocean anthropogenic carbon uptake through 2080.

2 Methods

2.1 Efficiency Metric and Historical Scaling

Efficiency, η, is k_M (Equation 2) referenced to the year ~~1990. This allows efficiency to be~~ 1990, and expressed as a percentage:

$$\eta(t) = \frac{k_M(t)}{k_M(1990)} \times 100 \tag{3}$$

Referencing k_M to 1990 values maximizes the time ocean anthropogenic carbon uptake is at 100% efficiency during the historical period, 1920-2006 (Figure S1). The historical scaling for ocean anthropogenic carbon air-sea flux (F_{ant}) is closely related to k_M :

$$\overset{*}{F}_{ant}(t) = k_M(1990) C_{ant}^{ATM}(t) = F_{ant}(1990) \frac{C_{ant}^{ATM}(t)}{C_{ant}^{ATM}(1990)} \tag{4}$$

The overset "*" notation indicates the variable that has been extrapolated with the historical scaling. Here, $F_{ant}(1990)$ is diagnosed from the CESM simulations. Following from Equation 3, ocean carbon sink efficiency (η) is related to the historical scaling:

$$\eta(t) = \frac{F_{ant}(t)}{\overset{*}{F}_{ant}(t)} \times 100 \tag{5}$$

Under the approximately exponential pCO_2^{atm} increase of the historical period, k_M is relatively constant, thus $F_{ant}(t) \approx \overset{*}{F}_{ant}(t)$ and historical period efficiency is ~100%. Because it is approximately equal to F_{ant}, $\overset{*}{F}_{ant}$ has been used to estimate historical $F_{ant}(t)$ (Lovenduski et al., 2008). In the future, as k_M declines from 1990 values, F_{ant} will be less than $\overset{*}{F}_{ant}(t)$, i.e. efficiency will decline. In this study, $\overset{*}{F}_{ant}(t)$, extrapolated into the future with projected pCO_2^{atm}, is taken as ~~an upper bound for~~ a useful reference point against which to compare projected future ocean anthropogenic carbon uptake.

We also use the historical scaling as a baseline for determining ~~ocean~~ anthropogenic carbon concentration ($C_{ant}(x,y,z,t)$) changes in the interior (Tanhua et al., 2007; Gruber et al., 2019) in CESM:

$$\overset{*}{C}_{ant}(x,y,z,t) = C_{ant}(x,y,z,1990)\frac{C^{ATM}_{ant}(t)}{C^{ATM}_{ant}(1990)} \quad (6)$$

We use reference anthropogenic carbon concentrations ($C_{ant}(x,y,z,1990)$) from the CESM simulations. The $C_{ant}(x,y,z,t)$ historical scaling exists because the exponential signal of atmospheric CO_2 increase is transmitted by the air-sea flux of anthropogenic carbon to surface ocean mixed layer anthropogenic carbon concentration (C^{ML}_{ant}), and then ocean circulation passes the exponential signal into the interior. C^{ML}_{ant} is closely related to the time integral of the air-sea flux of anthropogenic carbon (Section 2.3). ~~Therefore, because~~ Because the integral of an exponential is also an exponential, C^{ML}_{ant} has also increased exponentially. ~~The~~ From the surface, the exponential atmospheric signal is ~~then propagated~~ propagated to deeper layers by the ocean circulation~~to deeper layers. However, in the future, atmospheric signals will not be transferred directly to~~ .

With this work, we study the three processes that will cause the ocean carbon sink to diverge from its historical scaling in the coming decades, through 2080. First, the linear relationship between increasing C^{ML}_{ant} and pCO_2^{ocn} will end due to ~~a decreasing chemical~~ the decreasing buffer capacity for CO_2. Second, ~~the propagation of the exponential signal to depth by the ocean circulation is dependent on the vertical gradient of in the near-surface ocean. When~~ warming of the surface ocean will cause reduced CO_2 solubility. Third, if emissions are mitigated, ~~waters towards the surface will fallin concentration as atmospheric concentrations are reduced~~C^{ML}_{ant} will fall, but slightly deeper waters will still contain the higher C_{ant} concentrations set by the atmospheric CO_2 of decades prior. There will thus be a "back-pressure" on ~~the surface ocean concentration~~ C^{ML}_{ant} coming from near-surface water that ~~re-emerge~~ reemerge at the surface (Bopp et al., 2015; Iudicone et al., 2016). ~~Thus, future will deviate from $\overset{*}{C}_{ant}(x,y,z,t)$~~Our assessment of this back-pressure effect does not require change in the ocean circulation, as our decomposition assumes a circulation to be constant. Instead, this back pressure can be explained by the relatively slow rate at which the ocean redistributes C_{ant} from surface to depth.

2.2 Ocean Component of the Earth System Model

We use the Community Earth System Model 1 (Hurrell et al., 2013) for our analysis for our analysis of the three-dimensional ocean carbon sink. The CESM's ocean component model, POP2, provides the three-dimensional, time-evolving estimates of the ocean carbon cycle (Long et al., 2013). POP2 output is from publicly available CESM climate simulations provided by the National Center for Atmospheric Research (NCAR). POP2 features 60 vertical levels and a nominal 1° x 1° horizontal resolution. Surface boundary layer physics are parameterized using the K-Profile Parameterization (KPP) of Large et al. (1994). Unresolved advection by eddies is parameterized with the Gent-McWilliams parameterization (Gent and Mcwilliams, 1990). Isopycnal mixing is parameterized with the Redi (1982) diffusion operator. The biogeochemical output comes from the embedded Biogeochemical Elemental Cycle (BEC) model (Moore et al., 2004). Anthropogenic carbon concentration is calculated in the model as the difference between natural carbon, a tracer that experiences a fixed preindustrial pCO_2^{atm}, and contemporary carbon, a tracer that experiences time evolving pCO_2^{atm}.

~~All of the climate~~ Following a long preindustrial spin-up, all simulations used here are forced ~~with~~ for the historical period (1850-2005) with observations of pCO_2^{atm}. For 2006-2080, forcing is pCO_2^{atm} from the Representative Concentration Pathways (RCPs) or a 1.5°C scenario (Sanderson et al., 2017)~~from 2006-2080~~. For the ~~historical period, 1920-2005, simulations are forced with observations of . For the~~ 1.5°C scenario, a concentration pathway was designed that limited warming the CESM to 1.5°C, for the purpose of investigating avoided climate impacts (Sanderson et al., 2017). This scenario features the same forcing as RCP8.5 until 2017, except for CO_2. Unfortunately, the projected CO_2 forcing was not smoothly joined to the historical CO_2 forcing, creating a period of anomalously low anthropogenic carbon flux from 2006 to 2017 (Figure S2). To avoid this unrealistic feature in our main figures, we plot the 1.5°C scenario only after 2017.

Multiple CESM simulations are run with the same pCO_2^{atm} forcing to generate single model ensembles for each scenario. The ensemble approach allows for separation of internal variability from the forced signals, with the latter being the focus of this study. NCAR has run multiple ensembles with different forcings including CESM Large Ensemble (40 members, RCP8.5; Kay et al. (2015)), CESM Medium Ensemble (15 members, RCP4.5), and the CESM Low-Warming Ensemble (10 members, 1.5°C; Sanderson et al. (2017)). Individual ensemble members are branched off at 1920 (Kay et al., 2015). Ocean biogeochemistry output is limited to 9 members for the medium ensemble and the 3 for the low warming ensemble~~, thus we also only use~~. To ensure a comparable number of ensemble members across our analysis, we use only 9 ensemble members for ~~the~~ RCP8.5~~experiment~~.

In coupled climate models, historical climate variability of the carbon sink is not expected to match observations because the phasing of ENSO or other internal climate variability is different in each ensemble member. Averaging across an ensemble removes the imprint of internal variability to reveal the response to external forcing (Kay et al., 2015). With only a single coupled climate simulation, decadal means would typically be used to smooth internal climate variability. However, since we are using an ensemble mean in which this variability has already been removed, ~~a single year provides~~ the single years that we plot provide a snapshot of the climate response to external forcing. In ~~our results, CESM is~~ this study, these CESM ensembles are used for all maps and sections. ~~We tune the one-dimensional~~ As explained below, we tune the reduced-form model to replicate the CESM's air-sea CO_2 flux (F_{ant}) under each scenario, and then use the ~~one-dimensional~~ reduced-form model to decompose the mechanisms for future change in ~~efficiency of the global-mean ocean carbon sink~~ sink efficiency.

2.3 ~~One-Dimensional~~ Impulse Response Function Model for the Ocean Carbon ~~Cycle Model~~Sink

We employ an established ~~one-dimensional~~ reduced form ocean carbon cycle model based ~~in impulse response functions~~on an impulse response function (IRF). This model has been used for decades to emulate ocean carbon uptake simulated by complex ESMs (Joos et al., 1996; Raupach et al., 2014)~~. This same approach was also used~~, and is also used for all RCP scenarios to convert projected emissions to ~~convert emissions projections to the RCP4.5 and RCP8.5~~ CO_2 ~~concentration pathways~~ concentrations (Meinshausen et al., 2011).

Impulse response functions characterize the dynamic system response to small perturbations around a steady state, with the full response being the sum of infinite discrete pulses. For the global-mean ocean carbon cycle, a pulse of anthropogenic carbon added to the surface ocean by air-sea exchange and the impulse response function determines the timescale with which that

pulse moves to deeper ocean layers. Surface ocean anthropogenic carbon content is solved as the convolution integral of the air-sea flux (F_{ant}, the impulse) and the lifetime of that anthropogenic carbon pulse ($r(t)$, the impulse response function):

$$C_{ant}^{ML}(t) = \frac{1}{h}\frac{c}{h \cdot A_{oc}} \int_{t_i}^{t} F_{ant}(u) r(t-u) du \quad (7)$$

The ~~convolution integral~~ air-sea flux of anthropogenic carbon is dependent on the air-sea partial pressure gradient (ppm) and the gas exchange coefficient (k_g, yr^{-1}):

$$F_{ant} = k_g(pCO_2^{atm} - pCO_2^{ocn}) \quad (8)$$

Where pCO_2^{ocn} is the preindustrial pCO_2^{ocn} ($pCO_2^{ocn,PI}$) plus an anthropogenic perturbation (δpCO_2^{ocn}), including effects of changing buffer capacity and temperature (Appendix A). Forcings are the historical and projected pCO_2^{atm} that forced CESM, and historical and projected SST output by CESM.

The convolution integral in Equation 7 sets the concentration at time t by calculating the fraction of previous pulses ($F_{ant}(u)$), that entered the ocean mixed layer at times prior ($t_i = 0$ to t). The effective mixed layer depth, h is adjusted to tune the historical air-sea flux of anthropogenic carbon of the ~~one-dimensional~~ IRF model to emulate the historical ensemble-mean of CESM. ~~The optimal h is 109 m. The~~ CESM's historical flux is best replicated with h = 51m. We implement the impulse response function ($r(t)$) that was diagnosed by ~~Joos et al. (1996)~~ Joos et al. (1996, 2001) from the HILDA (HIgh Latitude-exchange/interior Diffusion-Advection) model. $r(t)$ is fixed in time, which is equivalent to assuming a constant ~~ocean circulation~~ circulation and background natural carbon cycle. There is a unit conversion factor (c = 1.722 μmol m^3 ppm^{-1} kg^{-1}); and A_{oc} is the ocean area (m^2).

~~The convolution integral (Equation 7)is derived from the model's surface anthropogenic carbon tendency equation:~~

~~$$\frac{\partial C_{ant}^{ML}}{\partial t} = \frac{F_{ant}}{h} + \frac{K_{z,eff}}{h}\frac{\partial C_{ant}^{ML}}{\partial z}$$~~

~~Integrating:~~

~~$$C_{ant}^{ML}(t) = \frac{1}{h}\int_0^t \left(F_{ant} + K_{z,eff}\frac{\partial C_{ant}^{ML}}{\partial z}\right) dt$$~~

~~Where $K_{z,eff}$ is the effective vertical diffusivity. The one-dimensional model's $K_{z,eff}$ must match that of the ocean component of the ESM being emulated (Gnanadesikan et al., 2015).~~ Directly diagnosing an ocean model's mixed layer impulse response function would require special simulations (Joos et al., 1996) ~~, and this is unnecessary~~that have not been performed for CESM. Instead, ~~with~~ we show below that with the IRF from HILDA and h as tuning parameter, ~~the diffusive anthropogenic carbon flux term can be estimated by difference from the other two terms (Oeschger et al., 1975; Meinshausen et al., 2011).~~ we can emulate CESM behavior both historically and under these three future scenarios (Figure 2d). Thus, we can use this IRF to assist in separating the mechanisms of ocean carbon sink change that are occurring in the CESM projections. It is important to note that despite the ability of the IRF model to emulate CESM behavior for our period of study, this does not mean it

should be expected to emulate CESM on longer timescales. Particularly under high emissions, greater ocean circulation and biogeochemical changes are expected beyond 2100 (Randerson et al., 2015).

~~Finally~~

2.4 Mechanistic Decomposition of the Air-Sea Flux

Considering anthropogenic perturbations on top of a background natural state in the surface ocean, the air-sea flux of anthropogenic carbon is ~~dependent on the air-sea partial pressure gradient and the gas exchange coefficient (m^{-2} yr^{-1})~~a function of the pCO_2 in the atmosphere and ocean (Equation 8), and pCO_2^{ocn} is a function of the anthropogenic carbon content (C_{ant}) and the temperature (T):

~~$F_{ant} = ck_g(pCO_2^{atm} - pCO_2^{ocn})$~~

$F_{ant}(pCO_2^{atm}, pCO_2^{ocn}(C_{ant}, T))$. Change in gas-exchange rates are assumed negligible, and because the biological pump is part of the background natural cycle, it is also assumed constant. The total derivative of the air-sea flux of anthropogenic carbon (Equation 8) can then be written in terms of its partial derivatives:

$$\frac{dF_{ant}}{dt} = \underbrace{\overbrace{\frac{\partial pCO_2^{atm}}{\partial t}}^{atm.\ gr.\ rate} \frac{\partial F_{ant}}{\partial pCO_2^{atm}}}_{atmos.\ component} - \underbrace{\overbrace{\frac{\partial pCO_2^{ocn}}{\partial t}}^{ocn.\ gr.\ rate} \frac{\partial F_{ant}}{\partial pCO_2^{ocn}}}_{ocean\ component} \tag{9}$$

~~A conversion factor, c, converts the flux units from ppm m^{-2} yr^{-1} to mmol m^{-2} yr^{-1}. We calculate~~

A positive pCO_2^{atm} ~~as the preindustrial~~ growth rate enhances F_{ant}, while positive pCO_2^{ocn} ~~($pCO_2^{ocn,PI}$) plus an anthropogenic perturbation (δpCO_2^{ocn}), including effects of changing buffer capacity and temperature (Appendix A). The remaining forcings are the historical and projected~~ growth acts to decrease F_{ant}. Since the pCO_2^{atm} ~~that forced CESM, and historical and projected SST output by CESM.~~ growth rate is prescribed, we further expand only the ocean component:

$$\frac{\partial pCO_2^{ocn}}{\partial t} = \frac{\partial C_{ant}}{\partial t}\frac{\partial pCO_2^{ocn}}{\partial C_{ant}} + \frac{\partial T}{\partial t}\frac{\partial pCO_2^{ocn}}{\partial T} \tag{10}$$

2.5 ~~Process Decomposition Using One-Dimensional Ocean Carbon Cycle Model Simulations~~

With the first term being the effect of the buffer factor and ocean circulation, and the second the sensitivity of pCO_2^{ocn} to warming via carbon chemistry. For the global-mean, the first term can be further separated using:

$$\frac{\partial C_{ant}}{\partial t} = F_{ant} + K_z \frac{\partial C_{ant}}{\partial z} \tag{11}$$

Where K_z is a vertical diffusivity representing the global-mean ocean circulation (Munk, 1966) acting on the vertical gradient of C_{ant} in the ocean.

Substituting Equation 11 into Equation 10, we arrive at three terms controlling the evolution of pCO_2^{ocn} :

$$\frac{\partial pCO_2^{ocn}}{\partial t} = \underbrace{F_{ant}\overbrace{\frac{\partial pCO_2^{ocn}}{\partial C_{ant}}}^{buffer\ factor}}_{impact\ of\ air-sea\ flux} + \underbrace{K_z\frac{\partial C_{ant}}{\partial z}\overbrace{\frac{\partial pCO_2^{ocn}}{\partial C_{ant}}}^{buffer\ factor}}_{impact\ of\ vertical\ C_{ant}\ transport} + \underbrace{\frac{\partial T}{\partial t}\overbrace{\frac{\partial pCO_2^{ocn}}{\partial T}}^{warm.\ sens.}}_{impact\ of\ warming} \tag{12}$$

On the right hand side, the first term is the impact of the air-sea flux on pCO_2^{ocn}, modulated by the buffer factor; the second the impact of ocean vertical transport, also modulated by the buffer factor, and the third the impact of warming on carbon chemistry. This conceptual decomposition is useful to understanding our experiments with the IRF model, explained in the following section.

2.5 Process Decomposition Using the Impulse Response Function Model

Table 1. ~~Description of the two experiments conducted~~ Experiments with the ~~one-dimensional carbon cycle~~ IRF model~~(Control and Constant Chemical Capacity)~~, ~~the~~ historical scaling~~experiment~~, and the effects quantified ~~from these experiments~~by differencing.

Experiment Name	Description	Symbol	Scenarios
All Effects (Control)	full chemistry, warming	~~ΔC_{total}~~ C_{total}	RCP8.5, RCP4.5, 1.5°C
Constant Temperature	constant temperature	C_{nowarm}	RCP8.5, RCP4.5, 1.5°C
Constant Chemical Capacity	constant buffer factor	~~ΔC_{ccc}~~ C_{ccc}	RCP8.5, RCP4.5, 1.5°C
Historical Scaling[1]	constant efficiency	~~$\Delta \overset{*}{C}_{hs}$~~ $\overset{*}{C}_{hs}$	RCP8.5, RCP4.5, 1.5°C

Effect Name	Effect Symbol	Equation
Warming	ΔC_{warm}	$C_{total} - C_{nowarm}$
Chemical Capacity	ΔC_{chem}	$C_{nowarm} - C_{ccc}$
Vertical Transport of C_{ant}	ΔC_{transp}	$C_{ccc} - \overset{*}{C}_{hs}$

1. ~~$\Delta \overset{*}{C}_{hs}$~~ $\overset{*}{C}_{hs}$ is calculated directly from pCO_2^{atm} (~~$\Delta \overset{*}{C}_{hs} = \int \overset{*}{F}_{ant}\, dt$~~ $\overset{*}{C}_{hs} = \int \overset{*}{F}_{ant}\, dt$; Equation 4)

In ~~addition to~~ CESM, F_{ant}, the vertical gradient of C_{ant}, the buffer factor, the circulation and the temperature are all evolving (Equation 12). Thus our emulation of CESM ~~(~~is the ΔC_{total} IRF experiment and it implicitly includes all these effects (Table 1; "All Effects (Control")~~, we~~ . We perform two sensitivity ~~experiments with the one-dimensional model for each scenario of future (Table 1). Cumulative change in the ocean anthropogenic inventory is denoted as ΔC_X~~ studies in which the temperature is held constant such that there are no impacts on carbon solubility, C_{nowarm} ("Constant Temperature"); and in which the buffer factor is held constant at a pre-industrial value and there is no warming, C_{ccc} ("Constant Chemical Capacity"). The cumulative anthropogenic carbon uptake consistent with the historical scaling for each scenario is ~~$\Delta \overset{*}{C}_{hs}$~~ $\overset{*}{C}_{hs}$, calculated directly from the prescribed pCO_2^{atm} (Table 1; Equation 4; "Historical Scaling"). Combining these experiments ~~,~~allows quantification of the

~~two~~ three negative effects, ΔC_{warm}, ΔC_{chem} and ~~ΔC_{cgrad}~~ΔC_{transp}, that combine to make ~~ΔC_{total}~~ C_{total} lower than the historical scaling (~~$\Delta \overset{*}{C}_{hs}$~~): ~~$\overset{*}{C}_{hs}$~~):

$$\Delta C_{total} = \Delta \overset{*}{C}_{hs} + \Delta C_{warm} + \Delta C_{chem} + \Delta C_{cgradtransp} \quad (13)$$

~~Changes~~ Since the circulation is assumed constant, the change due to warming, ΔC_{warm} only accounts for the impact of warming on solubility. Change in ocean chemical capacity, ΔC_{chem}, ~~are~~ is the change in anthropogenic carbon ~~in a one-dimensional~~ uptake in the IRF model simulation with ~~all effects, ΔC_{total}~~ full chemistry but no warming, C_{nowarm}, minus the change in anthropogenic carbon in ~~a one-dimensional~~ the IRF model simulation with ~~constant chemical capacity, ΔC_{ccc}~~ a constant buffer factor and no warming, C_{ccc} (Table 1). ~~The carbon gradient effect, ΔC_{cgrad}, is~~ Thus, ΔC_{chem} quantifies the impact of change in carbonate chemistry that occurs as additional C_{ant} is absorbed going forward. The impact of the vertical transport of C_{ant} from surface to depth and warming, ΔC_{transp}, is estimated as the difference between ΔC_{ccc} and the time integral of $\overset{*}{F}_{ant}$, ~~$\Delta \overset{*}{C}_{hs}$. The carbon gradient effect~~ $\overset{*}{C}_{hs}$, which is equivalent to solving Equation 13 for this term. The impact of the vertical transport of C_{ant} on the ocean sink is due to ~~interactions between the~~ the sensitivity of the transport of anthropogenic carbon ~~out of the surface ocean and the growth rate of~~ from surface to depth on the vertical profile of C_{ant} (Equation 12). The physical circulation ~~is~~ and background natural carbon cycle are assumed fixed in the ~~one-dimensional ocean carbon cycle~~ IRF model, consistent with ~~CESM not experiencing significant changes in circulation~~ the carbon cycle in CESM not illustrating significant sensitivity to such changes over 1920-2080 under RCP8.5 high-emission forcing (Randerson et al., 2015). However, we demonstrate ~~below that change in the carbon gradient on which this circulation acts will significantly impact the ocean carbon sink under scenarios of emission mitigation.~~

2.6 ~~Anthropogenic Carbon Air-Sea Flux Decomposition~~

~~We use the one-dimensional model to identify the dominant controls on ocean anthropogenic carbon uptake. The air-sea flux of anthropogenic carbon is a function of the p of the atmosphere and ocean (Equation 10),~~ here that in the scenario of aggressive mitigation, there is significant change in the vertical gradient of C_{ant} on which this circulation will act, and ~~is a function of the anthropogenic carbon content (and the temperature, T): $F_{ant}(pCO_2^{atm}, pCO_2^{ocn}(C_{ant}, T))$. Total derivative of the air-sea flux of anthropogenic carbon ($\frac{dF_{ant}}{dt}$) can be written in terms of its partial derivatives:~~

$$\frac{dF_{ant}}{dt} = \underbrace{\overbrace{\frac{\partial pCO_2^{atm}}{\partial t}}^{atm.\ gr.\ rate} \frac{\partial F_{ant}}{\partial pCO_2^{atm}}}_{atmos.\ component} - \underbrace{\overbrace{\frac{\partial pCO_2^{ocn}}{\partial t}}^{ocn.\ gr.\ rate} \frac{\partial F_{ant}}{\partial pCO_2^{ocn}}}_{ocean\ component}$$

~~The first term on the right is the impact of~~ thus the ~~growth rate (atmosphere component) and the second term is the impact of the growth rate (ocean component). Given Equation 10, $\frac{\partial F_{ant}}{\partial pCO_2^{atm}} = \frac{\partial F_{ant}}{\partial pCO_2^{ocn}}$, and thus variations in F_{ant} are solely due to variations in the and growth rate. The closely follows , with the same sign. A positive growth rate enhances F_{ant}, while positive growth acts to decrease F_{ant} (Equation 10). The growth rate is prescribed, and the ocean component is further~~

expanded:

$$\frac{\partial pCO_2^{ocn}}{\partial t} = \frac{\partial C_{ant}}{\partial t}\frac{\partial pCO_2^{ocn}}{\partial C_{ant}} + \frac{\partial T}{\partial t}\frac{\partial pCO_2^{ocn}}{\partial T}$$

net effect of $\Delta C_{transport}$ will be to slow the ocean carbon sink.

With the first term representing the effect of the buffer factor, and the second the sensitivity of to warming. Substituting in Equation 8, we arrive at three terms controlling ocean :

$$\frac{\partial pCO_2^{ocn}}{\partial t} = \underbrace{\frac{F_{ant}}{h}\overbrace{\frac{\partial pCO_2^{ocn}}{\partial C_{ant}}}^{buffer\ factor}}_{impact\ of\ air-sea\ flux} + \underbrace{\frac{K_{z,eff}}{h}\frac{\partial C_{ant}}{\partial z}\overbrace{\frac{\partial pCO_2^{ocn}}{\partial C_{ant}}}^{buffer\ factor}}_{impact\ of\ physical\ removal} + \underbrace{\frac{\partial T}{\partial t}\overbrace{\frac{\partial pCO_2^{ocn}}{\partial T}}^{warm.\ sens.}}_{impact\ of\ warming}$$

On the right hand side, the first term is the impact of the air-sea flux on , the second the impact of physical removal, and the third the impact of warming. With ocean circulation is constant in the one-dimensional model, the vertical carbon gradient is the key term for physical removal. Because the impact of warming is small through 2080, for our analysis the growth rate becomes a balance between the impact of the air-sea flux on and the carbon gradient. Air-sea flux acts to increase for all scenarios through 2100, thus the first term is always positive. The vertical gradient ($\frac{\partial C_{ant}}{\partial z}$) is always negative, thus this term always decreases .

In the ΔC_{total} experiment (Table 1), F_{ant}, the vertical gradient, the buffer factor, and sensitivity to warming all evolve (Equation 14). In the ΔC_{ccc} experiment, the buffer factor is fixed at a preindustrial value. The $\Delta \overset{*}{C}_{hs}$ experiment is equivalent to a constant buffer factor, a warming sensitivity of 0, and, as shown in the results, setting the anthropogenic carbon profile to that predicted by historical scaling.

3 Results

3.1 Projected Spatial Redistribution Patterns of the Anthropogenic Carbon Air-Sea Carbon Flux

From CESM, we diagnose the In CESM, the projected spatial distribution of the air-sea flux of anthropogenic carbon for from 2020-2080 differs across the three future scenarios: 1.5°C, RCP4.5, RCP8.5. Here we focus on the projected spatial distribution of the air-sea flux of anthropogenic carbon from 2020-2080.

In the 1.5°C scenario, the spatial pattern of the air-sea flux of anthropogenic carbon changes significantly from 2020-2080. While most of the ocean is a sink in 2020, in 2050 and 2080 there are large regions of anthropogenic carbon outgassing (Figure 1, bottom row). Most pronounced is the emergence of anthropogenic carbon outgassing in the equatorial Pacific. The outcrop region of Sub-Antarctic Mode Water (SAMW) at about 50°S also experiences outgassing by 2080. In 2020, the Kuroshio and subpolar North Atlantic are some of the most intense sinks of C_{ant}, but by 2080, these regions are sources. Contrastingly, Southern Ocean anthropogenic carbon uptake persists throughout the simulation.

In the RCP4.5 scenario, equatorial Pacific outgassing of anthropogenic carbon grows over time (Figure 1, middle row), but is less widespread and intense than in the 1.5°C scenario. The intensity of uptake flux decreases over time for the subpolar and

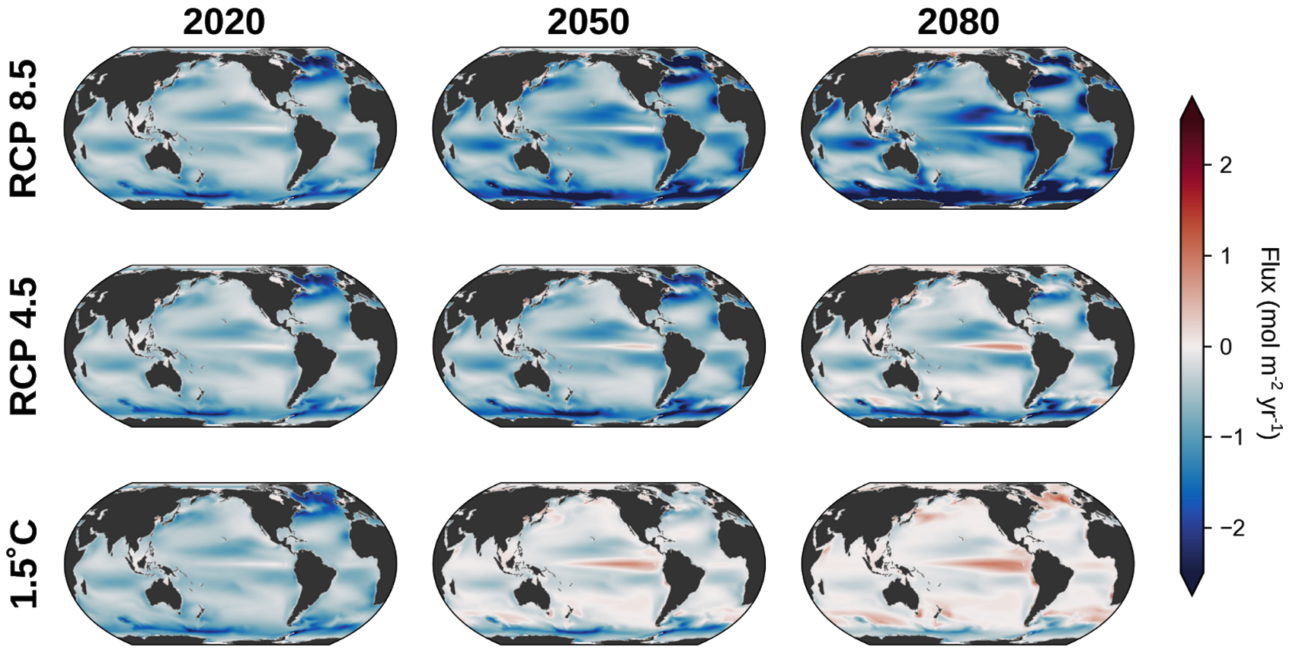

Figure 1. CESM ensemble-mean air-sea flux of anthropogenic carbon (mol C_{ant} m^{-2} yr^{-1}; positive = red = to the atmosphere). Each row is a scenario, and each column represents a year. Emission mitigation is greatest at the bottom of each column.

mid-latitude Atlantic and Kuroshio region. Beyond the equatorial Pacific, the spatial pattern of the air-sea flux of anthropogenic carbon is similar to the RCP8.5 scenario, but the amplitude of uptake is reduced.

Relative to the scenarios with emission mitigation (1.5°C and RCP4.5), the RCP8.5 scenario features a consistent spatial pattern of the air-sea flux of anthropogenic carbon (Figure 1, top row). The primary change over time is an amplification of magnitude, with the highest flux intensity occurring in 2080.

~~Globally-mean~~ Global-mean anthropogenic carbon fluxes across the air-sea interface are greatest in RCP8.5, and lowest in 1.5°C (Figure 2a). In the RCP4.5 scenario, the air-sea flux of anthropogenic carbon peaks in 2050, and then gradually declines. In the 1.5°C scenario, ocean anthropogenic carbon uptake peaks in 2020, and is almost zero by 2080. In all scenarios, the ocean anthropogenic carbon inventory increases through 2080 (Figure 2d).

Extrapolation of the ocean anthropogenic carbon uptake based on the historical scaling ($\overset{*}{F}_{ant}$) is dependent solely on pCO_2^{atm} (Equation 4). Lower pCO_2^{atm} results in a lower estimate of ocean anthropogenic carbon uptake, and higher pCO_2^{atm} results in ~~greater uptake~~a greater uptake estimate using the historical scaling. For all scenarios, CESM-simulated ~~air-sea~~ anthropogenic carbon uptake is far less than $\overset{*}{F}_{ant}$ (Figure 2a). Reduced uptake relative to $\overset{*}{F}_{ant}$ indicates that in the future, ocean anthropogenic carbon uptake will be less efficient than for the "historical scaling" (Figure 2b). Efficiency remains greater than 90% from 1990 through 2010, but then declines under all future scenarios, with greater efficiency declines as emission mitigation increases. The efficiency decrease is approximately linear in RCP8.5 and RCP4.5, but exponential in the 1.5°C scenario.

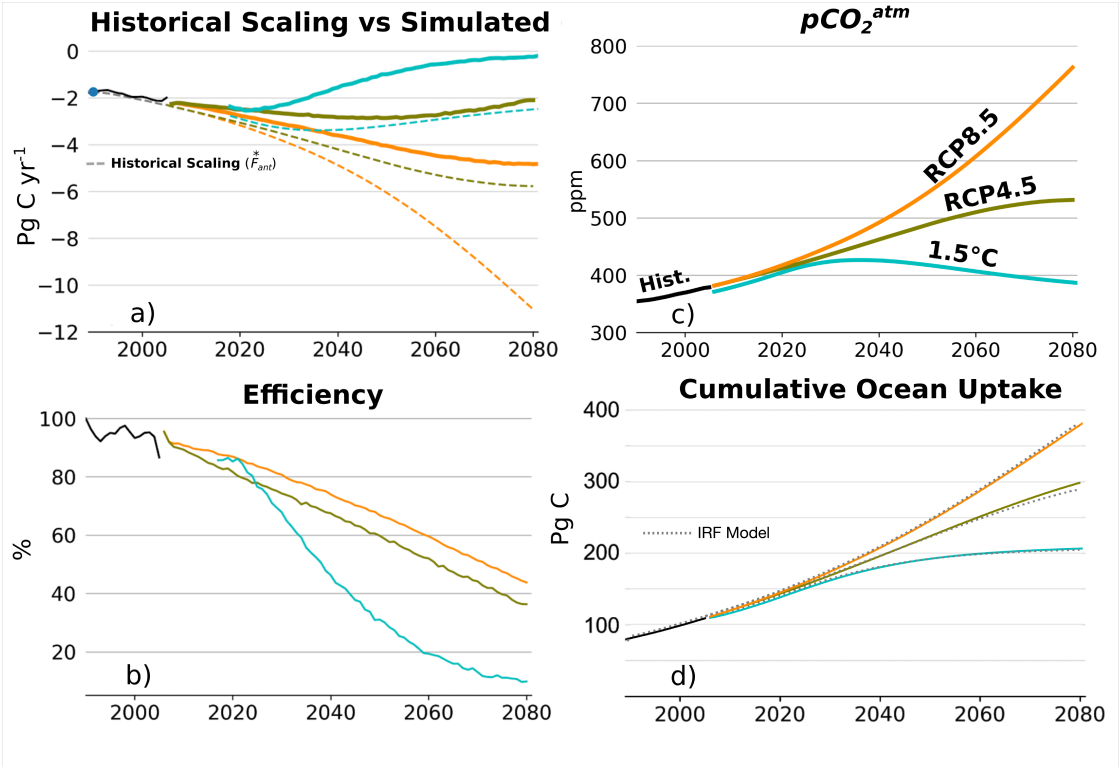

Figure 2. (a) Historical scaling of ocean anthropogenic carbon uptake ($\overset{*}{F}_{ant}$; dotted lines) and CESM anthropogenic carbon uptake (F_{ant}; solid lines) for three scenarios (1.5°C, RCP4.5, and RCP8.5). Negative indicates atmospheric anthropogenic carbon removal. (b) Efficiency of the global ocean sink for the three scenarios from CESM (Equation 5). (c) pCO_2^{atm} for both CESM and ~~one-dimensional~~ IRF model. (d) Total anthropogenic carbon accumulation in CESM (solid lines) and in the ~~one-dimensional~~ IRF model (dotted lines). Flux and efficiency from 2006-2017 are not shown for 1.5°C scenario due to ocean adjustment to pCO_2^{atm} forcing (see Methods 2.2; Figure S2).

The 1.5°C scenario is the only scenario with negative pCO_2^{atm} growth rates (Figure ~~2b), which substantially modifies the ocean carbon cycle response, as shown below~~2c).

3.2 Projected Changes in the Ocean Interior

Here, we analyze the evolution of the ~~anthropogenic carbon~~ C_{ant} vertical gradient by applying the historical scaling (Equation 6) to CESM's global-mean vertical profile of anthropogenic carbon ($C_{ant}(z)$). ~~Deviations are~~ In Figure 3 and 4, deviations from the historical scaling are quantified as $C_{ant}(z) - \overset{*}{C}_{ant}(z)$. Weakening of the vertical C_{ant} gradient reduces the strength of physical removal of anthropogenic carbon to depth ~~(Equation 14)~~ and reduces the ~~magnitude of the air-sea flux~~ accumulation of C_{ant} in the surface ocean (Equation 12). Wherever $C_{ant}(z) > \overset{*}{C}_{ant}(z)$, more carbon is stored at that ~~location~~ depth than predicted by the historical scaling and the deviation is positive. If deviations are reduced at the surface relative to the interior, the

vertical gradient is ~~weaker~~weakened, and thus ocean anthropogenic carbon uptake ~~less efficient than expected by the historical scaling~~is less efficient.

With more rapid emission mitigation, globally average profiles reveal increasingly positive deviations from the historical scaling at depth (Figure 3). For RCP8.5 and RCP4.5, $C_{ant}(z)$ increases from 2020-2080 at all depths, but at the surface, $C_{ant}(z)$ increases less than $\overset{*}{C}_{ant}(z)$ (Figure 3a). In the RCP4.5 scenario, the anthropogenic carbon below 200m is greater than $\overset{*}{C}_{ant}(z)$ (Figure 3b), while in the RCP8.5 scenario it is lesser (Figure 3a). In both RCP8.5 and RCP4.5, the increase in anthropogenic carbon is surface-intensified. The resulting enhanced vertical gradient allows for increased downward physical transport of C_{ant}, and thus increased ocean anthropogenic carbon uptake (Equation 12). However, the enhancement of the vertical gradient is not as strong as the historical scaling would suggest.

In the 1.5°C scenario, the largest change ~~fro~~ from 2020 to 2080 in $C_{ant}(z)$ is at depth; at the surface, anthropogenic carbon decreases less significantly (Figure 3c). This leads to a much weaker vertical gradient, weaker vertical transport, and thus a reduced ocean anthropogenic carbon uptake. The surface loss of anthropogenic carbon is a short-term response to declines in pCO_2^{atm} that begin in 2036, while the increase in ~~$C_{ant}(z)$~~ C_{ant} at depth is ~~from~~ attributable to the long-term increase in pCO_2^{atm} relative to preindustrial times~~driven by the large-scale ocean circulation~~, and the movement of this signal into the upper ocean through processes such as mode water formation (Bopp et al., 2015; Iudicone et al., 2016; Toyama et al., 2017).

The signals found in $C_{ant}(z)$ can also be identified in zonal-mean sections from CESM (Figure 4). In the RCP8.5 scenario (Figure 4, top row), the surface layer exhibits the strongest negative deviation from the historical scaling, but there is no positive deviation in the interior. The negative deviation is seen in deep waters between 25°N and 60°N, and also in the bowls of the northern and southern subtropical gyres. The negative deviation grows from 2020-2080, and appears to propagate into the ocean interior with NADW.

In the RCP4.5 scenario, the surface layer exhibits a growing negative deviation (Figure 4, middle). The negative surface deviation spans from the southern to the northern end of the zonal mean section. In the interior, however, there is a growing positive deviation. The positive deviation occurs because the ocean interior is not in contact with the atmosphere and thus the ocean circulation is circulating C_{ant} set by the ~~the~~ pCO_2^{atm} of ~~several decades~~~~previous~~prior decades. In other words, there is a lagged ~~response in the interior to the emission mitigation occurring in~~ interior response to RCP4.5 ~~,~~ in which pCO_2^{atm} growth ~~slows over time~~ gradually slows (Figure 2c).

The 1.5°C scenario features ~~large~~ even larger positive deviations from the historical scaling occurring throughout the thermocline (Figure 4, bottom row). As for RCP4.5, this occurs because ~~there is no mechanism by the~~ the rapid slowdown of pCO_2^{atm} ~~can be communicated to these waters. In other words, these waters hold on to the signals of higher from prior decades (Figure 2c). As these~~ is not immediately communicated to the interior. As thermocline waters outcrop in the equatorial Pacific and ~~mid~~ middle to high latitudes, they drive a source of anthropogenic carbon to the atmosphere (Figure 1).

3.3 Drivers of Simulated Changes in Efficiency

The ~~one-dimensional model faithfully~~ IRF model reasonably replicates the cumulative ocean uptake of CESM (Figure 2d), supporting the assumption of constant circulation and the use of parameterized chemistry ~~. The one-dimensional~~ in the IRF. The

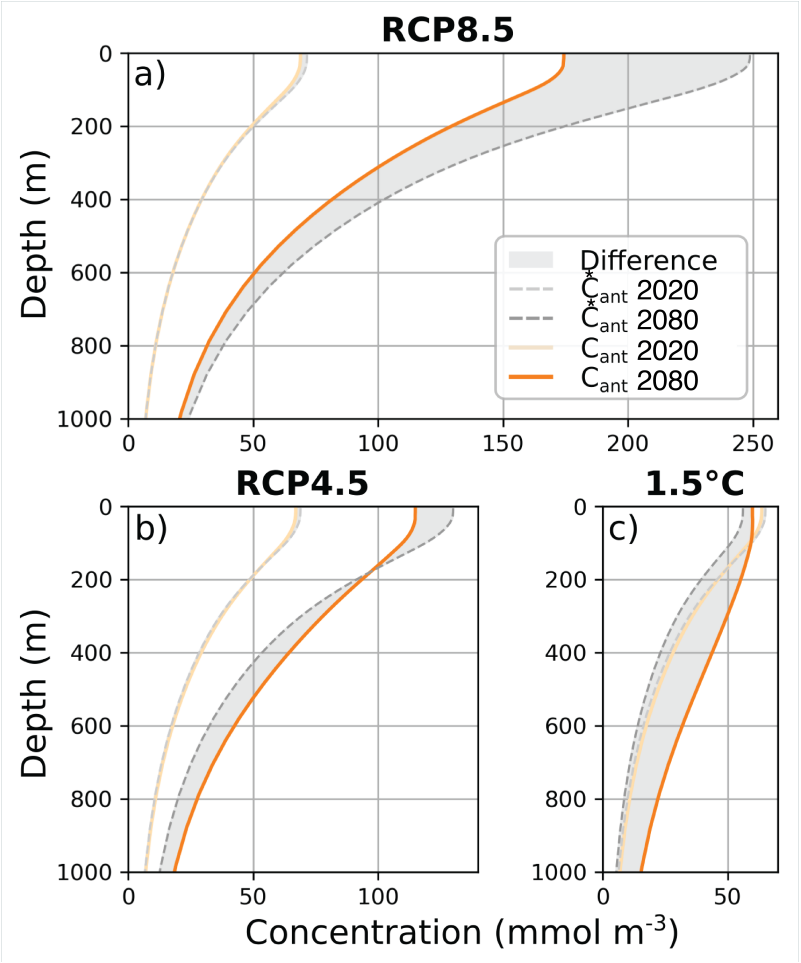

Figure 3. CESM global-mean anthropogenic carbon profiles ($C_{ant}(z)$) (orange, solid), and profiles of $\overset{*}{C}_{ant}(z)$ (gray, dashed), for the (a) RCP8.5 scenario, (b) RCP4.5 scenario, and (c) 1.5°C scenario. The shaded region between the dashed and solid lines indicates the deviation from the historical scaling. Light lines are for 2020 and dark lines are for 2080. The shaded region between the lines is shown for zonal mean sections in Figure 4.

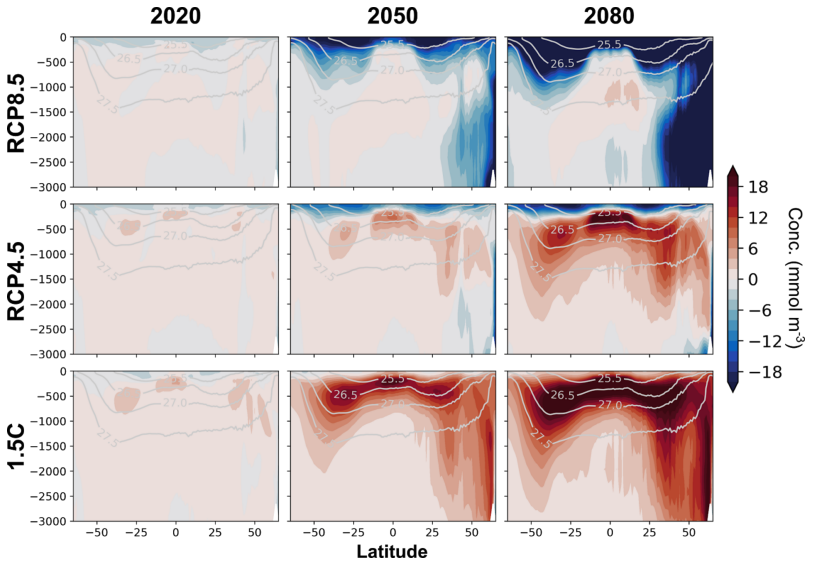

Figure 4. Ocean component model output of the global zonal mean deviation of anthropogenic carbon concentration (mmol m^{-3}) from the historical scaling of anthropogenic carbon ($C_{ant} - \overset{*}{C}_{ant}$). Rows and columns same as Figure 1. Positive regions indicate faster carbon accumulation than historical scaling, negative regions indicate slower accumulation. Contour lines are surfaces (kg m^{-3}).

IRF model can be ~~easily~~ manipulated for our sensitivity experiments (Table 1). With these experiments, a deeper mechanistic understanding of the changes in ocean carbon uptake efficiency simulated by CESM can be developed.

Over the historical ~~forcing period (1920-2006~~period (1920-2005), accumulation of carbon (ΔC_{total}) is nearly identical to the historical scaling (Figure 5)~~, with the difference between them attributable to ΔC_{cgrad}~~. This is consistent with previous findings of ~~a~~ the ocean sink being slightly ~~below~~ less the theoretical prediction of the historical scaling (Raupach et al., 2014).

~~In~~

Under RCP8.5, the ocean ~~cumulatively absorbs 393~~ absorbs 385 Pg anthropogenic carbon through 2080 (Figure 5, top~~) by 2080~~, black line), approximately 2.5 times the present-day anthropogenic carbon inventory (160-166 PgC_{ant}; ~~Devries~~DeVries, 2014). ~~In RCP8.5, the historical scaling tracks closely to the simulation with constant chemical capacity. If~~ Due to the fact that ocean chemical capacity ~~were to remain constant, the ocean would absorb 158~~ changes in the future, uptake is reduced significantly, -233 PgC_{ant} from 2020 to ~~2080. The slightly positive ΔC_{cgrad} is attributable to fitting CESM anthropogenic carbon uptake to 100% efficiency for 1990, despite the historical period having experienced slightly less than exponential . Changes in ocean anthropogenic carbon uptake due to warming are very small relative to ΔC_{chem}, making up <5% of the total efficiency decline, and thus these are not shown. This small contribution~~ 2080 from what it would be if the buffer factor were to remain constant (light blue shade). In addition to this limit on uptake due to chemistry, there is a small additional reduction due to warming, -20 PgC_{ant} (dark blue shade). The positive difference between C_{ccc} and the historical scaling (green line; +98PgC_{ant} by 2080) indicates that if the ocean were to have a fixed chemical capacity and were to experience no warming, it would be a substantially larger sink than estimated by the historical scaling. Exceeding the historical scaling is consistent with

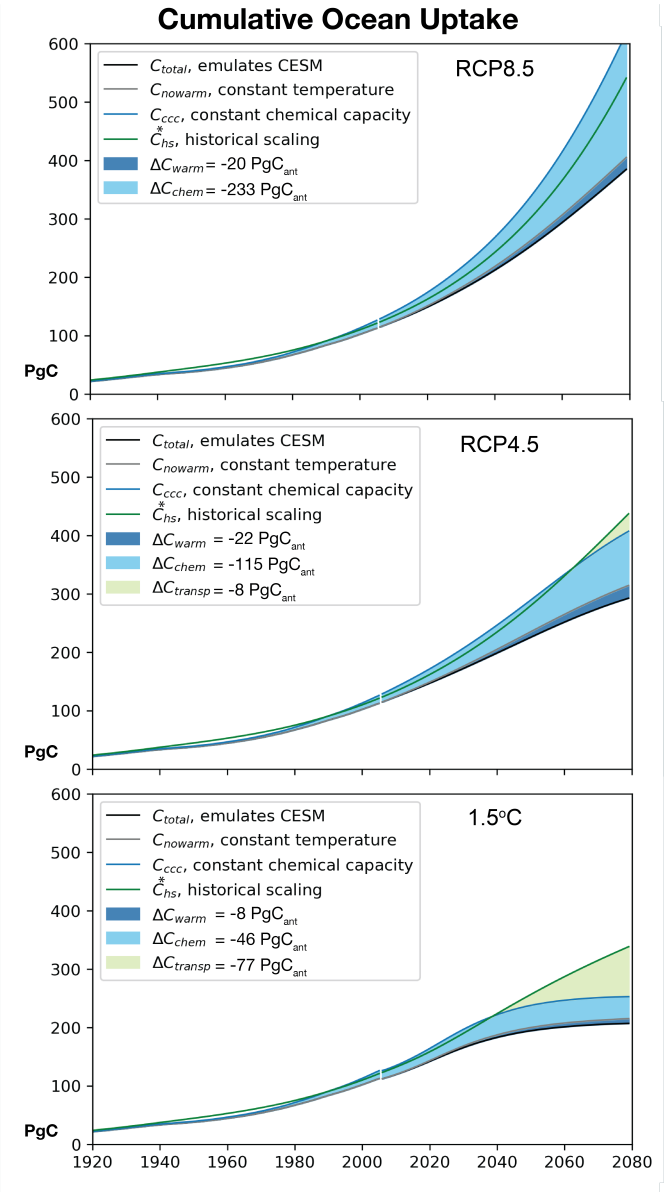

Figure 5. Cumulative ocean anthropogenic carbon uptake (PgC_{ant}) in the IRF model; historical and for three future scenarios. The green line is the historical scaling (C^*_{hs}). The dark blue line is the IRF model simulation of constant chemical capacity with no impact of warming on solubility (C_{ccc}). The gray line is the IRF simulation with no impact of warming on solubility (C_{warm}). The black line is the IRF model simulation that includes all effects (C_{total}), variable chemical capacity and warming impacts on solubility); this model replicates closely the cumulative carbon uptake of CESM (Figure 2d). Light green shading represents the residual, estimating the decrease in uptake related to vertical C_{ant} transport (ΔC_{transp}) for RCP4.5 and the 1.5°C scenario. Light blue shading represents decreases in uptake related to chemical capacity (ΔC_{chem}). Dark blue shading indicates the decrease due to warming impacts on solubility (ΔC_{warm}). For each scenario, the carbon uptake from 2020 to 2080 is indicated in the label, with negative indicating loss relative to the total potential uptake.

the ~~change due to warming calculated in~~ RCP8.5 pCO_2^{atm} having a trajectory that exceeds an exponential after 2012 (Figure S3). As in previous studies of climate-carbon feedbacks (Randerson et al., 2015; Schwinger and Tjiputra, 2018), we find that buffering is primarily responsible for limiting the ocean carbon uptake under high emissions scenarios through 2080, and that warming plays a secondary role.

~~Cumulative ocean anthropogenic carbon uptake (Pg C) in the one-dimensional model, historical and for three future scenarios. The cyan line is the extrapolation based on the historical scaling. The dark blue line is the one-dimensional model simulation of constant chemical capacity (PI buffer factor) with variable solubility. The black line is the one-dimensional model simulation that includes all effects (variable chemical capacity and variable solubility); this model replicates closely the cumulative carbon uptake of CESM (Figure 2d). Light green shading represents decreases in uptake related to the carbon gradient effect (ΔC_{cgrad}), teal shading represents decreases in uptake related to chemical capacity (ΔC_{chem}). For each scenario, the carbon uptake from 2020 to 2080 is indicated in the label, with negative indicating net loss.~~

~~In~~ Under RCP4.5, the ocean absorbs ~~307~~ 292 Pg anthropogenic carbon (Figure 5, middle~~) from 2020 to~~ , black line) through 2080. Cumulative uptake predicted by the historical scaling approximately tracks the constant chemical capacity ~~simulation until around 2040. After 2040, the historical scaling and the constant chemical capacity simulation diverge, indicating the increasing impactof the carbon gradient due to the decreasing growth rate of the forcing. The ΔC_{cgrad} effect amounts to -52 Pganthropogenic carbon in~~ through 2060. The impact of transport (light green shade), ΔC_{transp}, has only a small negative impact, -8 PgC_{ant} cumulatively through 2080. This combines with the stronger ΔC_{chem} effect ~~that amounts to -84 Pganthropogenic carbon by 2080. These two effects reduce the~~ (-115 PgC_{ant}), and the impact of warming on solubility (-22 PgC_{ant}). In total, the ocean carbon sink is reduced by a total of ~~31~~33% from the historical scaling, ~~with approximately 1/3 of the effect due to the vertical gradient and 2/3 due to~~ due mostly to carbonate chemistry.

~~In~~ Under the 1.5°C scenario, the ocean absorbs ~~213~~ 207 Pg anthropogenic carbon (Figure 5, bottom, black line) by 2080. ~~The~~ ΔC_{chem} ~~effect is the weakest in this scenario, -37 PgC in 2080. The weak~~ reduces uptake from the historical scaling (-46 PgC_{ant} in 2080), and the additional impact of warming is -8 PgC_{ant}. The weaker ΔC_{chem} effect than in the other scenarios is consistent with ~~this scenario taking up the least anthropogenic carbon because chemical capacity decreases as anthropogenic carbon uptake increases. ΔC_{cgrad}~~ the ocean taking up far less anthropogenic carbon in this scenario (Figure 2d). In contrast to the other scenarios, ΔC_{transp} (light green shade) is the dominant ~~change in this scenario~~factor that reduces carbon uptake from the historical scaling, accounting for ~~-90~~ -77 PgC_{ant}. The strongly reduced vertical gradient of anthropogenic carbon (Figure 3, 4) results in reduced vertical ~~anthropogenic carbon removal (Equation 8~~transport from surface to depth (Equation 12). For the 1.5°C scenario, the ocean carbon sink is reduced by ~~a total of 38~~39% from the historical scaling, with ~~approximately 2/3 of the effect due to the vertical gradient and 1/3 due~~ over half of this change due to vertical C_{ant} transport and the remainder due mostly to carbonate chemistry.

3.4 ~~Decomposition of the Anthropogenic Air-Sea Carbon Flux~~

~~In the one-dimensional model, the air-sea flux (F_{ant}) is controlled by large and opposing components, the atmosphere component, driven by the atmosphere growth rate, and the ocean component, driven by the ocean growth rate (Equation 12). Because F_{ant}~~

adds anthropogenic carbon to the surface, the impact of the air-sea flux is to increase . The impact of ocean circulation is to decrease given the downward vertical anthropogenic carbon gradient (Equation 14). Considering the atmosphere and ocean component terms separately offers additional insight into the drivers of F_{ant}.

(a-c) Global-mean air-sea flux of anthropogenic carbon, F_{ant}, (green line; Pgyr^{-1}), separated into its ocean (blue line; Pgyr^{-1}) and atmosphere (orange line; Pgyr^{-1}) components (Equation 12), for 1850-2080. Positive is a net carbon sink. In (d-f). the same terms are integrated from 2040 (vertical dashed line in (a-c)) and presented on a log scale to highlight the changing roles of the ocean and atmosphere components for different mitigation scenarios. Components are zero in 1850 (a-c) because there is no air-sea flux of at this time, but non-zero in (d-f) because there is an air-sea flux of in 2040.

In the RCP8.5 scenario, the atmosphere component acts to enhance F_{ant}, and the ocean component acts to reduce the air-sea flux (F_{ant}, Figure 6a,d). The actual F_{ant} (Figure 6, green) is a small residual of these tendencies, reaching up to 5 PgC yr^{-1} in 2080 (Figure 6a, inset). The steady increase in acts increases air-sea pCO_2 difference, and the resulting increasing acts to decrease F_{ant} (Equation 12). If did not rise in response to F_{ant}, such as the hypothetical scenario where the ocean were instantaneously well-mixed from surface to deep, ocean anthropogenic carbon uptake would have the enormous magnitude of the atmospheric component (Figure 6a-b). In fact, is driven up by both F_{ant} and reduced by the ocean circulation that moves carbon to depth.

In the RCP4.5 scenario, the atmosphere and ocean components acts similarly to the RCP8.5 scenario, with the atmosphere component enhancing and ocean component reducing F_{ant} (Figure 6b,e). As plateaus (Figure 2c) aroudn 2040, the atmospheric component reduces in magnitude. The ocean component also declines because of the less negative vertical gradient in the ocean (Figure 3,4). By 2040, the ocean effect overwhelms the the atmosphere component, leading to a less net uptake in 2080 than in 2040 (Figure 6e).

In the 1.5°C scenario, the atmosphere increasingly drives up F_{ant}, while the ocean component reduces F_{ant} until the early 21st century. By 2040, the tendencies in these F_{ant} components have switched (Figure 6c,f). Emission mitigation causes to plateau, and then to decrease slightly (Figure 2d). After 2040, the ocean sink is declining rapidly, and flux tendencies in the atmosphere and ocean component have switched (Figure 6f). As declines after 2040, the atmosphere component flux declines (Figure 6c,f). On the ocean side, the carbon gradient effects cause lesser removal, and thus the ocean is less able to mitigate growth of (Figure 6c,f). Consistent with the spatially resolved fluxes from CESM (Figure 1), the result is a strong reduction of the net flux.

4 Discussion

4.1 Drivers of Future Efficiency Declines

We use the CESM and a one-dimensional an IRF model that emulates the CESM's global-mean behavior to assess the mechanisms of future change in the ocean carbon sink as dependent on the future pCO_2^{atm} and ocean internal accumulation of anthropogenic carbon (C_{ant}). We show that the efficiency of ocean carbon uptake, i.e. how closely ocean carbon uptake follows the observed proportionality between uptake and atmospheric CO_2 (the "historical scaling"), will be reduced with rapid

CO_2 mitigationthat will cause reduced or negative growth rates of , . This finding is consistent with theory (Raupach et al., 2014) and past idealized modeling studies (Zickfeld et al., 2016; Schwinger and Tjiputra, 2018).

We show that the dominant mechanisms of efficiency decline differ across the three scenarios for future pCO_2^{atm}. With roughly exponential above-exponential growth of pCO_2^{atm} in RCP8.5, the strong increase of C_{ant}^{ML} concentrations causes a reduced chemical capacity that dominates the reduction of in efficiency (Figure 5, top). At the same time, this strong increase of causes a strong vertical carbon gradient to be a strong surface to depth gradient of C_{ant} is maintained (Figure 33a, 4)which supports , supporting continued downward transport of carbon to the ocean interior . Reversal of this vertical carbon gradient (Figure 3)dominates the reduction of efficiency in the (Equation 12). In RCP4.5, chemical capacity is also the dominant driver of the reduced sink, but a weakened vertical C_{ant} gradient allows transport to begin to play a role after 2060 (Figure 5, middle). In the 1.5°C scenario(Figure , a significant weakening of the vertical gradient of C_{ant} (Figure 3c) dominates the reduction in efficiency (Figure 5, bottom). Ocean sink efficiency for RCP4.5 is influenced both by the chemical capacity and the carbon gradient effects. Through 2080 for all scenarios, warming effects are negligibly small compared to the carbon gradient and chemical capacity effects.

With emission mitigation, the vertical carbon gradient gradient of C_{ant} does not immediately adjust to the trajectory of pCO_2^{atm}. Anthropogenic carbon accumulation from 2020-2080 is greatest in the thermocline,; a behavior that has been identified in other simulations of strong mitigation (Tokarska et al., 2019). This accumulation weakens the vertical carbon gradient gradient of C_{ant} (Figure 3, 4) and reduces the downward transport of C_{ant}. The bolus of anthropogenic carbon held at depth essentially creates a "back-pressure" that resists additional flow of anthropogenic carbon into the interior. If emissions are aggressively As emissions are mitigated, the larger the back-pressure effect (Figure 3-6grows (Figure 3-5). As the magnitude of the air-sea flux of anthropogenic carbon is fundamentally limited by the rate of surface anthropogenic carbon removal to depth transport of C_{ant} (Graven et al., 2012), slower removal to depth results in a reduced carbon uptake from the atmosphere.

Regionally, advective fluxes are important drivers of anthropogenic carbon reemergence (Bopp et al., 2015), thus the regional impacts of ocean circulation on ocean circulation impacts pCO_2^{ocn} (Equation 14) include the effects of through advection and watermass transformation . Surface waters of regions that trend towards anthropogenic carbon outgassing under emission mitigation (Figure 1; bottom row) are renewed connection to intermediate waters that are much older than the waters that renew the waters of the subtropics (Toyama et al., 2017). In the outgassing regions (Figure 1, bottom row), advective fluxes bring waters with an increasing load of anthropogenic carbon to the surface , increasing . Advection of anthropogenic carbon is driving the air-sea flux of anthropogenic carbon further towards outgassing (Bopp et al., 2015; Toyama et al., 2017). Advection returns to the surface waters that have already absorbed C_{ant}, and if the pCO_2^{atm} is falling when these waters remerge, the surface ocean carbon content will exceed the atmosphere and outgassing will occur. For the 1.5°C scenario, this occurs in the equatorial Pacific, supbolar subpolar and mid-latitude North Atlantic, SAMW outcrop region, and the Kuroshio (Toyama et al., 2017Figure 1 bottom). However, Circumpolar Deep Water (CDW) that is upwelled into the surface waters of the subtropics are renewed with waters that are shallower than where significant C_{ant} accumulation occurs, and surface waters of the Southern Ocean south of 50°S is old and largely uncontaminated by are renewed with deep waters without any C_{ant}, so its upwelling does not create the back-pressure effect. Because of the reemergence of . Thus, in some parts of the subtropics and Southern

Ocean, C_{ant} ~~, mitigation can be expected to result in substantial shifts of~~ uptake continues even with emissions mitigation while there is C_{ant} outgassing elsewhere. Particularly under aggressive emission mitigation, substantial shifts in the regional patterns of ~~the~~ air-sea carbon fluxes can be expected. These shifting patterns will need to be taken into account when planning for carbon cycle monitoring and diagnosis (Peters et al., 2017).

~~Reduced efficiency of the ocean carbon sink will occur independent of the emission scenario through 2080.~~

Whether before or after 2080, eventually ~~fossil field~~ emissions will decline either due to ~~mitigation~~ purposeful mitigation efforts or to the exhaustion of fossil fuel reservoirs. For example, ~~if~~ under the RCP8.5 scenario~~is followed into the 22nd century, future~~ , emissions would be flat from 2100 to 2150 and then decline dramatically (van Vuuren et al., 2011). ~~Thus, the carbon gradient~~ The back-pressure effect ~~will eventually come into play , even for the high emission scenario~~due to the vertical gradient of C_{ant} in the ocean will be delayed as long as pCO_2^{atm} is rapidly growing, but it will eventually play a role in reducing the ocean carbon sink. The longer mitigation is delayed, the greater the load of ~~anthropogenic carbon~~ C_{ant} in the thermocline will be, and thus the back-pressure effect will be larger in magnitude and temporal duration. ~~Climate~~ More climate simulations extending beyond 2100 are needed to quantify the back-pressure effect ~~in high emission~~ under all scenarios. Limiting emissions now makes it possible to reduce the eventual magnitude of the back-pressure effect and also to avoid the ocean chemistry changes that will additionally slow future ocean carbon uptake (Figure 4, 5).

4.2 Validity of the Model Representations of Ocean Physics

The back-pressure from anthropogenic carbon at depth is an unavoidable consequence of emission mitigation. How long the ocean will remain a net sink depends on the strength of the back-pressure effect, which depends on the ~~strength of surface ocean anthropogenic carbon removal. Thus, it is important to consider~~ how fast anthropogenic carbon is removed from the surface ocean to depth. This makes the fidelity of the ocean physics represented in ~~our one-dimensional model and also in the CESMthat it emulates.~~

~~Our one-dimensional ocean carbon cycle~~ the CESM, and then fit with the IRF model, very important. The IRF model represents multiple physical processes that remove carbon to depth as ~~a single diffusive process that is constant in time(Equation 8) using an effective vertical diffusivity, $K_{z,eff}$. The value for this term in the one-dimensional model~~ the decay of of a surface flux over time. This decay has been set (Section 2.3) so as to mimic advective, eddy-diffusive and watermass transformation processes occurring in CESM. Iudicone et al. (2016) show that advection and diabatic processes in watermass transformation are most important to the storage of C_{ant} in the mode waters of the upper ocean. ~~Thus, we wish to emphasize that the actual physical processes being emulated in the one-dimensional model with the effective diffusivity, $K_{z,eff}$, are primarily advective and diabatic.~~

For the historical period, ~~changes to ocean~~ global-mean air-sea fluxes and anthropogenic carbon storage ~~caused by differences in modeled ocean circulation are relatively small (Winton et al., 2013; Bronselaer and Zanna, 2020; Hauck et al., 2020),~~ are not substantially different across three-dimensional models, despite these models having substantial differences in the ocean circulation (Winton et al., 2013; McKinley et al., 2016; Bronselaer and Zanna, 2020; Hauck et al., 2020). This result is consistent with the external forcing from the growth of atmospheric pCO_2 being the overwhelming driver of the historical sink

(McKinley et al., 2020). Looking forward to a changing atmospheric boundary condition that is no longer increasing approximately exponentially, uncertainties in the ocean circulation, as indicated by the spread of model predictions for ocean heat uptake (Bronselaer and Zanna, 2020), may become important. For this study, we focus on evaluating the mechanisms in operation in CESM, but ~~recognize that~~ if we were emulating the ~~mean state of another ocean model, the findings may differ. A valuable direction for future work will be to evaluate the spread in predictions for these feedbacks.~~

~~As warming increases, the magnitude of climate-carbon feedbacks related to ocean circulation are likely to increase. We use our one-dimensional model to estimate climate-carbon feedbacks for CESM. The strength of ocean climate-carbon feedbacks (γ_o) in CESM is weaker (-2.4 Pg C K^{-1}) than the CMIP5 multi-model mean (-7.8 Pg C K^{-1}) (Arora et al., 2013; Friedlingstein, 2015) . For CESM, decline in ocean carbon uptake due to climate-carbon feedbacks in high emission scenarios is an order of magnitude smaller than due to change in ocean chemistry (Randerson et al., 2015). Though our one-dimensional model only includes the reduced solubility component of this feedback, the total response is quite close to the total CESM response (Figure 2d). This indicates that warming effects are not dominant in CESM prior to 2080. The remainder of the climate-carbon feedback is related is due to changing physical transport, which in the one-dimensional model is due only to the vertical carbon gradient and ocean circulation is constant. In simulations out the year 2300 with CESM (Randerson et al., 2015), or simulations with models featuring a rapidly declining AMOC (Sarmiento and LeQuéré, 1996), AMOC collapse does play a large role in reducing ocean carbon uptake. The small effect of changing ocean circulation in our simulation is likely because AMOC has yet to collapse by 2080 (Randerson et al., 2015). While assuming that climate-carbon feedbacks related to ocean circulation are small~~ ocean component of a different ESM, findings will likely be quantitatively different. Though assuming that change in the ocean circulation has a small impact on the carbon cycle prior to 2080 is consistent with the behavior of the CESM under RCP8.5 (Randerson et al., 2015), this may not be hold true for other ESMs or the real Earth. ~~It is important that the divergence of ESM estimates for the ocean carbon sink and its relationship to ocean circulation be assessed for a range of emissions scenarios~~A valuable direction for future work will be to evaluate the spread in predictions for both chemistry and vertical transport effects.

5 Conclusion

Atmospheric CO_2 has grown exponentially over the industrial era, and so has ocean anthropogenic carbon concentration at depth (DeVries, 2014; Gruber et al., 2019). Under ~~the~~ an exponential forcing regime, ocean anthropogenic carbon uptake also grows exponentially~~and,~~. Since these conditions have held over the historical era, ~~maintains~~ the ocean sink has historically maintained a high efficiency. In future scenarios, regardless of the degree to which emissions are mitigated by 2080, efficiency of ocean anthropogenic carbon uptake will decline. ~~However,~~ We show that the mechanisms of this decline will differ depending on the degree of mitigation. In the RCP8.5 ~~business-as-usual scenario~~and RCP4.5 scenarios, reduced buffer capacity explains ~~nearly all~~ most of the loss in ~~efficiency of ocean anthropogenic carbon uptake by 2080, 158 Pg C. In the case of scenarios with emission mitigation , such as RCP4.5 and~~ ocean sink efficiency through 2080. With strong mitigation in the 1.5°C scenario,

the loss of efficiency is due more to the ~~carbon gradient effect. The carbon gradient effect explains 38% of the efficiency loss in RCP4.5 scenario, and 71%~~ vertical transport of C_{ant}, which explains more than half of the efficiency loss~~in the 1.5°C scenario~~.

~~Changes~~ Change in the vertical anthropogenic carbon concentration gradient ~~are responsible for this carbon gradient effect. Under exponential growth, with constant chemical capacity and constant solubility, the vertical anthropogenic carbon gradient behaves as a function of , thus the air-sea flux of anthropogenic carbon behaves as though it is solely a function of , rather than a function of ,~~ is responsible for the changing impact of vertical transport of C_{ant}~~, and temperature~~ on the ocean sink. When emissions are mitigated and the growth in pCO_2^{atm} slows, the surface ocean carbon content responds rapidly. However, the ocean interior anthropogenic carbon concentration response lags the surface response. Below 100m in the ~~rapid mitigation~~ 1.5°C scenario, anthropogenic carbon concentration increases from 2020-2080; but above 100m, the anthropogenic carbon concentration ~~decreases. Thus the~~ begins to decrease starting in 2038, just two years after the maximum pCO_2^{atm} of 437ppm is achieved. The downward anthropogenic carbon concentration gradient is greatly reduced and there is less effective downward transport of C_{ant}. Ocean anthropogenic carbon uptake is limited by ~~surface ocean anthropogenic carbon removal (Graven et al., 2012), and thus the carbon gradient effect leads to lesser uptake~~ the removal of anthropogenic carbon from surface to depth (Graven et al., 2012). As the vertical gradient changes in the future~~relative to ocean anthropogenic carbon uptake under~~ , this transport is reduced and there will be less future uptake relative to what occurred at the same pCO_2^{atm} concentration in the historical period ~~.~~ (Schwinger and Tjiputra, 2018).

~~Under emission mitigation, the carbon gradient effect results in a enhanced outgassing of anthropogenic carbon in the equatorial Pacific, and a transition from anthropogenic carbon uptake to anthropogenic carbon outgassing in the subpolar and mid-latitude North Atlantic, Kuroshio, and SAMW outcrop region. These regions are hotspots for reemergence of mode waters (Bopp et al., 2015; Iudicone et al., 2016; Toyama et al., 2017) with high anthropogenic carbon contents. Waters of the subtropics are renewed with waters that are shallower where significant accumulation occurs, and the surface waters of the Southern Ocean are renewed with deep waters without any . Thus, in subtropics and Southern Ocean, the air-sea anthropogenic carbon uptake continues even with emissions mitigation.~~

The upper ocean circulation will play a critical role in the efficiency of the ocean carbon sink as the pCO_2^{atm} growth rate begins to slow. Current ocean model estimates of the ocean carbon sink agree well for the global-mean carbon uptake (Hauck et al., 2020) and future estimates under high emission scenarios do not diverge substantially ~~(Arora et al., 2013; Bronselaer and Zanna, 2020~~ ~~, which is consistent with our finding that the sink is not strongly dependent on the ocean circulation under exponential growth. Current ocean ocean circulation simulations, however, do diverge substantially~~ through 2100 (Arora et al., 2013). However, these simulations do diverge in their predictions of recent and near-future heat uptake, a process that is much more dependent on ~~the circulation simulation~~ circulation details (Bronselaer and Zanna, 2020). This suggests that for scenarios of aggressive emission mitigation, model predictions of the ocean carbon sink may diverge ~~substantially~~ much more than in the high emissions scenarios that have been the ~~focus of most modeling studies~~ primary focus to date (Friedlingstein et al., 2013; Randerson et al., 2015). Next steps will be to determine how much these simulations do diverge, and then to work to reduce these uncertainties. The ocean carbon sink plays a critical role in the global carbon cycle and the climate. Accurate predictions of its magnitude under all plausible future scenarios for pCO_2^{atm} are essential.

Code and data availability. The code used to run the IRF model is provided by the authors in a GitHub repository (https://qoccm.readthedocs.io/en/latest/). Raw output from the coupled ocean model simulations can download from NCAR's Earth System Grid (https://www.earthsystemgrid.org/).

Appendix A: ~~One-Dimensional~~ Ocean Carbon Cycle Model Carbon Chemistry for the Impulse Response Function Model

The pCO_2^{ocn} of the ~~one-dimensional~~ IRF ocean carbon cycle model is calculated using the empirical fit to the a solution of the carbonate system equations by Joos et al. (2001). We use a fitted solution for two reasons. First, when variables other than temperature and carbon are held constant, using the full carbonate system equations provides no additional accuracy. Second, the concentration scenarios used in CMIP5 (RCP4.5, RCP8.5) with which we wish to be consistent were generated using the same ~~one-dimensional~~ IRF model with the same representation of ocean chemistry.

$$pCO_2^{ocn} = [pCO_2^{ocn,PI} + \delta pCO_2^{ocn}(C_{ant}, T_{pi})]exp(\alpha_T \delta T) \tag{A1}$$

Where $pCO_2^{ocn,PI}$ is the preindustrial global-mean pCO_2^{ocn}. The response of pCO_2^{ocn} to warming is parameterized as an exponential function as in Takahashi et al. (1993), with α_T set to 0.0423 K^{-1}. The carbonate chemistry that determines δpCO_2^{ocn} given anthropogenic carbon (C_{ant}^{ML}) is parameterized assuming a fixed ocean alkalinity of 2300 μmol kg^{-1} and the preindustrial temperature, T_{pi}, based on an empirical fit to carbonate system calculations (Equation A24; Joos et al. (2001))

$$\delta pCO_2^{ocn}(C_{ant}, T_{pi}) = C_{ant}[A1 + C_{ant}(A2 + C_{ant}(A3 + C_{ant}(A4 + C_{ant}A5)))] \tag{A2}$$

With coefficients :

$$A1 = (1.5568 - 1.3993 \times 10^{-2} \times T_{pi}) \tag{A3}$$

$$A2 = (7.4706 - 0.20207 \times T_{pi}) \times 10^{-3} \tag{A4}$$

$$A3 = -(1.2748 - 0.12015 \times T_{pi}) \times 10^{-5} \tag{A5}$$

$$A4 = (2.4491 - 0.12639 \times T_{pi}) \times 10^{-7} \tag{A6}$$

$$A5 = -(1.5468 - 0.15326 \times T_{pi}) \times 10^{-10} \tag{A7}$$

Author contributions. Both authors contributed to the discussion and the writing of the paper

Competing interests. The authors declare that no competing interests are present

Acknowledgements. We would like to thank the National Science Foundation Division of Ocean Sciences (OCE-1948624 and OCE-1818501), NASA Earth Sciences Division (NNX/17AK19G), and Columbia University for funding this research. We would also like to thank Jared Lewis and Bodeker Scientific for sharing their pySCM (python Simple Climate Model, https://github.com/bodekerscientific/pyscm/) code on GitHub. This code provided the basis the ~~one-dimensional~~ IRF ocean carbon cycle model presented here. We acknowledge the CESM Large Ensemble Community Project and supercomputing resources provided by NSF/CISL/Yellowstone. This material is based upon work supported by the National Center for Atmospheric Research, which is a major facility sponsored by the National Science Foundation under Cooperative Agreement No. 1852977. We thank all the scientists, software engineers, and administrators who contributed to the development of CESM.

References

Arora, V. K., Boer, G. J., Friedlingstein, P., Eby, M., Jones, C. D., Christian, J. R., Bonan, G., Bopp, L., Brovkin, V., Cadule, P., Hajima, T., Ilyina, T., Lindsay, K., Tjiputra, J. F., and Wu, T.: Carbon-concentration and carbon-climate feedbacks in CMIP5 Earth system models, Journal of Climate, 26, https://doi.org/10.1175/JCLI-D-12-00494.1, 2013.

Bopp, L., Lévy, M., Resplandy, L., and Sallée, J. B.: Pathways of anthropogenic carbon subduction in the global ocean, Geophysical Research Letters, 42, 6416–6423, https://doi.org/10.1002/2015GL065073, 2015.

Bronselaer, B. and Zanna, L.: Heat and carbon coupling reveals ocean warming due to circulation changes, Nature, pp. 1–21, https://doi.org/10.1038/s41586-020-2573-5, 2020.

Canadell, J. G., Le Quéré, C., Raupach, M. R., Field, C. B., Buitenhuis, E. T., Ciais, P., Conway, T. J., Gillett, N. P., Houghton, R. A., and Marland, G.: Contributions to accelerating atmospheric CO2 growth from economic activity, carbon intensity, and efficiency of natural sinks, Proceedings of the National Academy of Sciences of the United States of America, 104, 18 866–18 870, https://doi.org/10.1073/pnas.0702737104, 2007.

DeVries, T.: The oceanic anthropogenic CO_2 sink: Storage, air-sea fluxes, and transports over the industrial era, Global Biogeochemical Cycles, 28, 631–647, https://doi.org/10.1002/2013GB004739, 2014.

Fassbender, A. J., Sabine, C. L., and Palevsky, H. I.: Nonuniform ocean acidification and attenuation of the ocean carbon sink, Geophysical Research Letters, 44, 8404–8413, https://doi.org/10.1002/2017GL074389, 2017.

Friedlingstein, P.: Carbon cycle feedbacks and future climate change, Philosophical Transactions of the Royal Society A: Mathematical, Physical and Engineering Sciences, 373, 20140 421, https://doi.org/10.1098/rsta.2014.0421, 2015.

Friedlingstein, P., Meinshausen, M., Arora, V. K., Jones, C. D., Anav, A., Liddicoat, S. K., and Knutti, R.: Uncertainties in CMIP5 Climate Projections due to Carbon Cycle Feedbacks, Journal of Climate, 27, 511–526, https://doi.org/10.1175/JCLI-D-12-00579.1, 2013.

Friedlingstein, P., Jones, M. W., O'Sullivan, M., Andrew, R. M., Hauck, J., Peters, G. P., Peters, W., Pongratz, J., Sitch, S., Quéré, C. L., Bakker, D. C. E., Canadell, J. G., Ciais, P., Jackson, R. B., Anthoni, P., Barbero, L., Bastos, A., Bastrikov, V., Becker, M., Bopp, L., Buitenhuis, E., Chandra, N., Chevallier, F., Chini, L. P., Currie, K. I., Feely, R. A., Gehlen, M., Gilfillan, D., Gkritzalis, T., Goll, D. S., Gruber, N., Gutekunst, S., Harris, I., Haverd, V., Houghton, R. A., Hurtt, G., Ilyina, T., Jain, A. K., Joetzjer, E., Kaplan, J. O., Kato, E., Klein Goldewijk, K., Korsbakken, J. I., Landschützer, P., Lauvset, S. K., Lefèvre, N., Lenton, A., Lienert, S., Lombardozzi, D., Marland, G., McGuire, P. C., Melton, J. R., Metzl, N., Munro, D. R., Nabel, J. E. M. S., Nakaoka, S.-I., Neill, C., Omar, A. M., Ono, T., Peregon, A., Pierrot, D., Poulter, B., Rehder, G., Resplandy, L., Robertson, E., Rödenbeck, C., Séférian, R., Schwinger, J., Smith, N., Tans, P. P., Tian, H., Tilbrook, B., Tubiello, F. N., Werf, G. R. v. d., Wiltshire, A. J., and Zaehle, S.: Global Carbon Budget 2019, Earth System Science Data, 11, 1783–1838, https://doi.org/10.5194/essd-11-1783-2019, 2019.

Gammon, R. H., Cline, J., and Wisegarver, D.: Chlorofluoromethanes in the northeast Pacific Ocean: Measured vertical distributions and application as transient tracers of upper ocean mixing, Journal of Geophysical Research: Oceans, 87, 9441–9454, https://doi.org/10.1029/JC087iC12p09441, 1982.

Gent, P. R. and Mcwilliams, J. C.: Isopycnal Mixing in Ocean Circulation Models, Journal of Physical Oceanography, 20, 150–155, https://doi.org/10.1175/1520-0485, 1990.

Gnanadesikan, A., Pradal, M.-A., and Abernathey, R.: Isopycnal mixing by mesoscale eddies significantly impacts oceanic anthropogenic carbon uptake, Geophysical Research Letters, 42, 4249–4255, https://doi.org/10.1002/2015GL064100, 2015.

Graven, H. D., Gruber, N., Key, R., Khatiwala, S., and Giraud, X.: Changing controls on oceanic radiocarbon: New insights on shallow-to-deep ocean exchange and anthropogenic CO_2 uptake, Journal of Geophysical Research: Oceans, 117, https://doi.org/10.1029/2012JC008074, 2012.

Gruber, N., Clement, D., Carter, B. R., Feely, R. A., van Heuven, S., Hoppema, M., Ishii, M., Key, R. M., Kozyr, A., Lauvset, S. K., Lo Monaco, C., Mathis, J. T., Murata, A., Olsen, A., Perez, F. F., Sabine, C. L., Tanhua, T., and Wanninkhof, R.: The oceanic sink for anthropogenic CO_2 from 1994 to 2007, Science, https://doi.org/10.1126/science.aau5153, 2019.

Hauck, J., Zeising, M., Le Quéré, C., Gruber, N., Bakker, D. C. E., Bopp, L., Chau, T. T. T., Gürses, Ö., Ilyina, T., Landschützer, P., Lenton, A., Resplandy, L., Rödenbeck, C., Schwinger, J., and Séférian, R.: Consistency and Challenges in the Ocean Carbon Sink Estimate for the Global Carbon Budget , Frontiers in Marine Science, 7, 3167, https://doi.org/10.3389/fmars.2020.571720, 2020.

Hausfather, Z. and Peters, G. P.: Emissions - the 'business as usual' story is misleading., Nature, 577, 618–620, https://doi.org/10.1038/d41586-020-00177-3, 2020.

Hurrell, J. W., Holland, M. M., Gent, P. R., Ghan, S., Kay, J. E., Kushner, P. J., Lamarque, J. F., Large, W. G., Lawrence, D., Lindsay, K., Lipscomb, W. H., Long, M. C., Mahowald, N., Marsh, D. R., Neale, R. B., Rasch, P., Vavrus, S., Vertenstein, M., Bader, D., Collins, W. D., Hack, J. J., Kiehl, J., and Marshall, S.: The Community Earth System Model: A Framework for Collaborative Research, Bulletin Of The American Meteorological Society, 94, 1339–1360, https://doi.org/10.1175/BAMS-D-12-00121.1, 2013.

Iudicone, D., Rodgers, K. B., Plancherel, Y., Aumont, O., Ito, T., Key, R. M., Madec, G., and Ishii, M.: The formation of the ocean's anthropogenic carbon reservoir, Scientific Reports, https://doi.org/10.1038/srep35473, 2016.

Joos, F., Bruno, M., Fink, R., Siegenthaler, U., Stocker, T. F., Quéré, C. L., and Sarmiento, J. L.: An efficient and accurate representation of complex oceanic and biospheric models of anthropogenic carbon uptake, Tellus B, 48, 397–417, https://doi.org/10.1034/j.1600-0889.1996.t01-2-00006.x, 1996.

Joos, F., Prentice, I. C., Sitch, S., Meyer, R., Hooss, G., Plattner, G.-K., Gerber, S., and Hasselmann, K.: Global warming feedbacks on terrestrial carbon uptake under the Intergovernmental Panel on Climate Change (IPCC) Emission Scenarios, Global Biogeochemical Cycles, 15, 891–907, https://doi.org/10.1029/2000GB001375, 2001.

Kay, J. E., Deser, C., Phillips, A., Mai, A., Hannay, C., Strand, G., Arblaster, J. M., Bates, S. C., Danabasoglu, G., Edwards, J., Holland, M., Kushner, P., Lamarque, J.-F., Lawrence, D., Lindsay, K., Middleton, A., Munoz, E., Neale, R., Oleson, K., Polvani, L., and Vertenstein, M.: The Community Earth System Model (CESM) Large Ensemble Project: A Community Resource for Studying Climate Change in the Presence of Internal Climate Variability, Bulletin of the American Meteorological Society, 96, 1333–1349, https://doi.org/10.1175/BAMS-D-13-00255.1, 2015.

Khatiwala, S., Primeau, F., and Hall, T.: Reconstruction of the history of anthropogenic CO_2 concentrations in the ocean, Nature, 462, 346–349, https://doi.org/10.1038/nature08526, 2009.

Large, W. G., McWilliams, J. C., and Doney, S. C.: Oceanic vertical mixing: A review and a model with a nonlocal boundary layer parameterization, Reviews of Geophysics, 32, 363–403, https://doi.org/10.1029/94RG01872, 1994.

Long, M. C., Lindsay, K., Peacock, S., Moore, J. K., and Doney, S. C.: Twentieth-Century Oceanic Carbon Uptake and Storage in CESM1(BGC), Journal of Climate, 26, 6775–6800, https://doi.org/10.1175/JCLI-D-12-00184.1, 2013.

Lovenduski, N., Gruber, N., and Doney, S.: Toward a mechanistic understanding of the decadal trends in the Southern Ocean carbon sink, Global Biogeochem. Cycles, 22, https://doi.org/10.1029/2007GB003139, 2008.

McKinley, G. A., Pilcher, D. J., Fay, A. R., Lindsay, K., Long, M. C., and Lovenduski, N. S.: Timescales for detection of trends in the ocean carbon sink, Nature, 530, 469–472, https://doi.org/10.1038/nature16958, 2016.

McKinley, G. A., Fay, A. R., Eddebbar, Y. A., Gloege, L., and Lovenduski, N. S.: External Forcing Explains Recent Decadal Variability of the Ocean Carbon Sink, AGU Advances, 1, e2019AV000 149, https://doi.org/10.1029/2019AV000149, 2020.

Meinshausen, M., Smith, S. J., Calvin, K., Daniel, J. S., Kainuma, M. L. T., Lamarque, J.-F., Matsumoto, K., Montzka, S. A., Raper, S. C. B., Riahi, K., Thomson, A., Velders, G. J. M., and van Vuuren, D. P.: The RCP greenhouse gas concentrations and their extensions from 1765 to 2300, Climatic Change, 109, 213, https://doi.org/10.1007/s10584-011-0156-z, 2011.

Moore, J. K., Doney, S. C., and Lindsay, K.: Upper ocean ecosystem dynamics and iron cycling in a global three-dimensional model, Global Biogeochemical Cycles, 18, https://doi.org/10.1029/2004GB002220, 2004.

Munk, W. H.: Abyssal recipes, Deep-Sea Res., pp. 707–730, https://doi.org/10.1016/0011-7471(66)90602-4, 1966.

Oeschger, H., Siegenthaler, U., Schotterer, U., and Gugelmann, A.: A box diffusion model to study the carbon dioxide exchange in nature, Tellus, 27, 168–192, https://doi.org/10.1111/j.2153-3490.1975.tb01671.x, 1975.

Peters, G. P., Le Quéré, C., Andrew, R. M., Canadell, J. G., Friedlingstein, P., Ilyina, T., Jackson, R. B., Joos, F., Korsbakken, J. I., McKinley, G. A., Sitch, S., and Tans, P.: Towards real-time verification of CO_2 emissions, Nature Climate Change, 7, 848–850, https://doi.org/10.1038/s41558-017-0013-9, 2017.

Randerson, J., Lindsay, K., Munoz, E., Fu, W., Moore, J., Hoffman, F., Mahowald, N., and Doney, S.: Multicentury changes in ocean and land contributions to the climate-carbon feedback: Carbon Cycle Feedbacks to 2300 in CESM, Global Biogeochemical Cycles, 29, https://doi.org/10.1002/2014GB005079, 2015.

Raupach, M. R., Gloor, M., Sarmiento, J. L., Canadell, J. G., Frölicher, T. L., Gasser, T., Houghton, R. A., Le Quéré, C., and Trudinger, C. M.: The declining uptake rate of atmospheric CO_2 by land and ocean sinks, Biogeosciences, 11, 3453–3475, https://doi.org/10.5194/bg-11-3453-2014, 2014.

Redi, M. H.: Oceanic Isopycnal Mixing by Coordinate Rotation, Journal of Physical Oceanography, 12, 1154–1158, https://doi.org/10.1175/1520-0485, 1982.

Sanderson, B. M., Xu, Y., Tebaldi, C., Wehner, M., O'Neill, B., Jahn, A., Pendergrass, A. G., Lehner, F., Strand, W. G., Lin, L., Knutti, R., and Lamarque, J. F.: Community climate simulations to assess avoided impacts in 1.5 and 2C futures, Earth System Dynamics, 8, 827–847, https://doi.org/10.5194/esd-8-827-2017, 2017.

Sarmiento, J. L. and LeQuéré, C.: Oceanic Carbon Dioxide Uptake in a Model of Century-Scale Global Warming, Science, 274, 1346–1350, https://doi.org/10.1126/science.274.5291.1346, 1996.

Schwinger, J. and Tjiputra, J.: Ocean Carbon Cycle Feedbacks Under Negative Emissions, Geophysical Research Letters, 45, 5062–5070, https://doi.org/10.1029/2018GL077790, 2018.

Takahashi, T., Olafsson, J., Goddard, J. G., Chipman, D. W., and Sutherland, S. C.: Seasonal variations of CO2 and nutrients in the high-latitude surface oceans: A comparative study, Global Biogeochem. Cycles, 7, 843–878, https://doi.org/10.1029/93GB02263, 1993.

Tanhua, T., Körtzinger, A., Friis, K., Waugh, D. W., and Wallace, D. W. R.: An estimate of anthropogenic CO_2 inventory from decadal changes in oceanic carbon content, Proceedings of the National Academy of Sciences, 104, 3037–3042, https://doi.org/10.1073/pnas.0606574104, 2007.

Tokarska, K. B., Zickfeld, K., and Rogelj, J.: Path Independence of Carbon Budgets When Meeting a Stringent Global Mean Temperature Target After an Overshoot, Earth's Future, 7, 1283–1295, https://doi.org/10.1029/2019EF001312, 2019.

Toyama, K., Rodgers, K. B., Blanke, B., Iudicone, D., Ishii, M., Aumont, O., and Sarmiento, J. L.: Large Reemergence of Anthropogenic Carbon into the Ocean's Surface Mixed Layer Sustained by the Ocean's Overturning Circulation, Journal of Climate, 30, 8615–8631, https://doi.org/10.1175/JCLI-D-16-0725.1, 2017.

van Vuuren, D. P., Edmonds, J., Kainuma, M., Riahi, K., Thomson, A., Hibbard, K., Hurtt, G. C., Kram, T., Krey, V., Lamarque, J.-F., Masui, T., Meinshausen, M., Nakicenovic, N., Smith, S. J., and Rose, S. K.: The representative concentration pathways: an overview, Climatic Change, 109, 5, https://doi.org/10.1007/s10584-011-0148-z, 2011.

Winton, M., Griffies, S. M., Samuels, B. L., Sarmiento, J. L., and Froelicher, T. L.: Connecting Changing Ocean Circulation with Changing Climate, Journal of Climate, 26, 2268–2278, https://doi.org/10.1175/JCLI-D-12-00296.1, 2013.

Zickfeld, K., Macdougall, A. H., and Matthews, H. D.: On the proportionality between global temperature change and cumulative CO_2 emissions during periods of net negative CO_2 emissions, Environmental Research Letters, 11, 055 006, https://doi.org/10.1088/1748-9326/11/5/055006, 2016.